Arab American University

Faculty of Graduate Studies

**Assessment of image quality and lesion detection in liver
spectral computed tomography based on image reconstruction
algorithms and virtual tube voltage**

By

Areej Ahmad Mohammad Hamami

Supervisor

Dr. Mohammed Al Jamal

**This thesis was submitted in partial fulfillment of the
requirements for the Master's degree in computed tomography
and magnetic resonance imaging sciences
February /2025**

Thesis Approval

Assessment of image quality and lesion detection in liver spectral computed tomography based on image reconstruction algorithms and virtual tube voltage

By

Areej Ahmad Mohammad Hamami

This thesis was defended successfully on 20/2/2025 and approved by:

Committee members   Signature

1. Dr. Mohammad Aljamal: Supervisor
2. Dr. Abed Alnasir Alasi: Internal Examiner
3. Dr. Osama Khodrog: External Examiner

Declaration

First and foremost, I am grateful to God for this accomplishment and to my family, who have always been there for me through all kinds of circumstances. I couldn't have accomplished anything without their support and encouragement. Your sacrifices and faith in me have inspired me to achieve my goals. I express my gratitude to all who wished me luck and prosperity. You have always been my beacon, and I appreciate that. With endless thanks and feelings, I dedicate this work to you.

Student Name: Areej Ahmad Mohammad Hamami

ID: 202113030

Signature:

Date of Submitting the Final Version of the Thesis: 23-04-2025

Acknowledgment

I want to express deep thanks to my family for their unwavering support during my academic journey. Your love, encouragement, and understanding have been my constant sources of motivation. Without the efforts that you made and your belief in me, this thesis would not have been possible.

My thesis supervisor, Dr. Mohammed Al Jamal, has greatly appreciated their professional guidance, tolerance, and knowledge. Thanks to your encouraging words, this work has taken on the most beautiful form. I appreciate the chances you gave me to develop and learn. I would like to express my gratitude to the doctors whose expertise and interest in sharing their knowledge have helped me better understand. Your guidance has had a significant impact on the trajectory of my career.

The support and friendship of my colleagues and radiography technicians have helped to make the difficulties easier to handle and the successes more significant. My love for this profession has grown due to our shared experiences, and I value the bond we have developed. Finally, I would like to thank everyone whose names may not be listed here but who helped me accomplish this thesis. Your encouragement, belief in me, and support have been invaluable. This work is presented to each of you with much gratitude.

Abstract

Introduction

The diagnostic capability of the radiological examination device is crucial for improving the diagnostic accuracy of liver disease. Spectral Detector Computed Tomography (SDCT) Innovation has shown high diagnostic performance in the assessment of liver diseases with better image quality compared to conventional computed tomography devices. Choosing the proper tube voltage and reconstruction algorithm type is crucial for maintaining image quality; improper settings can lead to increased noise and a reduced signal-to-noise ratio.

Purpose

Firstly this study aimed to evaluate the diagnostic accuracy of spectral CT. Secondly assessing image quality enhancement based on different virtual tube voltages and reconstruction algorithms for diagnosing common liver diseases.

Methods

This study is retrospective. Sixteen patients had previously been scanned by spectral CT and diagnosed with one of the following liver-related conditions: fatty liver, hemangiomas, or metastatic lesions. The virtual tube voltage and reconstruction algorithm were evaluated to assess the effect of tube voltage and algorithm type on the diagnostic efficiency of liver diseases in Spectral CT images. Images were reconstructed with different reconstruction algorithms such as iDose and IMR at various degrees with different virtual tube voltages. Three experienced radiologists analyzed eight combinations of reconstructed CT images, reviewing 128 scans from 16 patients.

Result

Among liver diseases, the signal-to-noise ratio was the highest among spectral CT images scanned with the IMR3 algorithm in metastatic, hemangioma, and fatty liver images. Nevertheless, when imaging abnormal liver lesions, SNR for all reconstruction techniques increases as tube voltage decreases.

Conclusion

Significant improvements were observed in several image quality metrics in SDCT when using low radiation doses. A specified strength of Iterative Reconstruction (IR) substantially enhanced signal-to-noise ratio (SNR) values for both normal and pathological liver tissues.

Table of Contents

List of Tables

List of Figures

Figure #	Title of Figure	Page

List of Appendices

List of Definitions of Abbreviations

Abbreviations	Title
AI	Artificial Intelligence
CAD	Computer-Aided Diagnosis
CC	Cholangiocarcinoma
CCA	cholangiocarcinoma
CCBD	Cloud Computing and Big Data
CM	Contrast Medium
CMS	Cystadenoma with Mesenchymal Stroma
CNR	Contrast-to-Noise Ratio
CT	computed tomography
CTDI	Computed Tomography Dose Index
CTPA	CT pulmonary Angiography
DECT	Dual-Energy Computed Tomography
DL	Deep Learning
DLCT	Dual-Layer Spectral Detector Computed Tomography
DLIR	Deep Learning Image Reconstruction
DLP	Dose-Length Product
DSCT	Dual-Source Computed Tomography
EHE	Epithelioid Angioendothelioma
FBP	Filtered Back Projection
FNH	Focal Nodular Hyperplasia

HA	Hepatic Abscess
HA	Hepatic adenoma
HCA	Hepatocellular Adenoma
HCC	Hepatocellular Carcinoma-
HEHE	Hepatic EHE
HH	Hepatic Hemangioma
HIR	Hybrid Iterative Reconstruction
HSCR	High Spatial Contrast Resolution
HU	Hounsfield Unit
HMH	Hepatic Mesenchymal Hamartoma
iCCA	Intrahepatic Cholangiocarcinoma
IMR	Iterative Model Reconstruction
IR	Iterative Reconstruction
IUR	Iodine Uptake Ratio
IV	Intravenous
LDH	Lactate Dehydrogenase
LUAD	Lung Adenocarcinoma
MEMBE	Model-Based Iterative Reconstruction
MDCT	Multi-Detector Computed Tomography
MonoE	Mono-Energy
MRI	Magnetic Resonance Imaging
MSAD	Multiple Scan Average Dose

NAFLD	Non-Alcoholic Fatty Liver Disease
nHCC	Necrotic Hepatocellular Carcinoma
NLP	Natural Language Processing
PACS	Picture Archiving And Communication System
PCLD	Polycystic Liver Disease
pNENs	Pancreatic Neuroendocrine Neoplasms
PNT	Partial Nodular Transformation
ROI	Region Of Interest
SD	Standard Deviation
SDCT	Spectral Detector Computed Tomography
SFOV	Scan Field Of View
SNR	Signal-to-Noise Ratio
US	Ultrasound
VMI	Virtual Monochromatic
WHO	World Health Organization

Chapter One: Introduction

1.1 Background

The liver is a massive, strong organ that helps the body with numerous vital processes. One of its most crucial roles is its ability to remove poisons from blood. Although the liver is well-suited for this task, the waste it breaks down exposes it to danger. The resources and capacity of the liver might be exhausted by an excessive amount of chemicals. This may occur momentarily or over an extended length of time (Gowda et al., 2009). Physicians from all specialties frequently deal with incidentally discovered abnormalities in liver function testing.

A large number of these patients lack main liver illness since the majority of the indicators often carried out are not liver-specific and are influenced by numerous variables not connected to liver disease. Additionally, a lot of liver enzyme levels, for example, are not a measure of the function of the liver but are indicators of damage to the liver, the purpose of liver blood tests is to provide proof that abnormalities, such as inflammation or damage to liver cells, have occurred or are occurring in the liver.

A thorough historical analysis, clinical assessment, and pattern interpretation. Any abnormalities in liver tests can frequently determine the type and causes of liver disease, enabling a focused method of investigation. When medical professionals talk about liver disease, they typically mean long-term illnesses that slowly destroy the liver. Common causes of chronic liver disease include metabolic disorders, toxic poisoning, and viral infections (Agrawal et al., 2016).

Due to the increasing use of medical imaging, asymptomatic lesions, especially benign, are being accidentally identified more frequently (Belghiti et al., 2014). The most common solid benign lesions are hepatocellular adenoma and focal nodular hyperplasia

(FNH), while hemangiomas and angiomyolipoma are mesenchymal in origin. With an estimated incidence of 3–20%, hepatic cavernous hemangiomas are the most frequent liver lesions, accounting for more than 70 of all benign liver lesions (Toro et al., 2014).

A fatty liver buildup of triglycerides in the liver that is greater than 5% of the liver weight is referred to as fatty liver. Non-alcoholic fatty liver disease (NAFLD) is the term for fatty liver without a diagnosis of alcohol consumption. In the world, NAFLD is a frequent form of long-term liver disease (Vernon et al., 2011).

The liver has the unpleasant distinction of receiving blood from both the systemic and portal circulations, giving it a dual blood supply. Since the liver is the first capillary bed that metastasizing cells contact and the hepatic sinusoids are fenestrated, allowing tumor cells to establish themselves and develop, hepatic metastases from gastrointestinal tract malignancies are frequent. 15% of patients with extra-abdominal tumors including bronchogenic carcinoma, 4% of patients with breast cancer, and 48% of patients with malignant melanoma had liver metastases as their initial site (Tsilimigras et al., 2021).

Also, several benign entities that may appear as metastases on multi-detector computed tomography (MDCT) are also caused by the dual blood supply to the liver such as focal fatty deposition (Gore et al., 2012). Much overlap in the HU values makes it difficult to characterize and distinguish between these tissues (Majeed et al., 2021).

The liver contributes to the production of proteins and the metabolism of lipids, carbohydrates, and amino acids in several intricate but crucial ways. A breakdown in one of these metabolic pathways is typically the fundamental pathophysiology of widespread parenchymal liver disorders. There are three types of parenchymal diseases: vascular, inflammatory, and storage. The assessment of diffuse liver disease involves the use of crosssectional hepatic imaging methods, particularly multidetector computed tomography (CT) and magnetic resonance imaging (MR).

Multidetector CT's significant function is largely characterized by its superior morphologic visualization capabilities, particularly about diffuse or focal intrahepatic lesions and the anatomical linkages between the liver and surrounding organs. From similarly sized and evenly spaced detector arrays to asymmetric detector arrangements, the wide range of available multidetector CT scanners results in imaging protocols with distinct parameters for nearly every multidetector CT system.

Emerging methods like dual-energy CT can be used for hepatic multidetector CT in addition to 64-detector row imaging. So the first workup of focal and diffuse liver disease frequently uses computed tomography (CT) because it is easy to tolerate, produces few artifacts in the images, and allows for a fast imaging of the entire abdomen and pelvis in one breath-hold (Boll and Merkle, 2009). Individual differences in the physiologic attenuation of liver parenchyma with unenhanced multidetector CT range from 55 to 65 HU. The normal liver parenchyma typically shows up as homogeneous on multidetector CT, and its attenuation is roughly 10 HU more than the spleen's.

The variable quantity of fat and glycogen accounts for the comparatively broad interindividual variation in hepatic attenuation; although more diffuse deposition of fat results in decreased attenuation, increasing glycogen is reflected as enhanced attenuation. Moreover, storage disorders involving iron or copper as deposited metabolites cause the hepatic parenchyma to attenuate more. Intrahepatic multidetector CT–opaque bile duct concretions can be identified with the aid of unenhanced multidetector CT. Hemorrhage that is parenchymal or subcapsular can also be recognized (Craig et al., 1989).

In contrast to angiographic examination that may be achieved by administering precisely timed minimal amounts of contrast agent in blood vessels, optimal liver imaging typically necessitates reliable contrast-enhancement of the liver parenchyma and the entirety of the hepatic circulation, including the artery, portal vein, and hepatic veins. This can only be accurately achieved by administering relatively high doses of intravenous (IV), contrast material quickly. It is especially crucial to use sufficiently high IV contrast doses

over multiphase scanning to detect and characterize liver abnormalities, including metastases and hepatocellular carcinoma-(HCC). To ensure that HU readings are directly comparable between phases of a liver exam, it is helpful to utilize the same kVp parameter for each phase (Kulkarni et al., 2021b).

Wide detector CT systems suffer from low contrast resolution, higher scatter, heel effect, cone beam defects, and a trade-off between spatial resolution & image noising because of the broad cone beam angle. A newer 3D anti-scatter grid has been introduced by several CT manufacturers to minimize the detrimental impact on image quality. Widedetector systems have demonstrated promising outcomes in cardiovascular domains; however, further research is necessary to determine their utility for other applications, which include liver scanning (Ramirez-Giraldo et al., 2015).

Spectral detector computed tomography (SDCT) has been found to enhance contrastto-noise ratio (CNR) and subjective image quality in low keV images for the evaluation of liver diseases such as cysts and hypovascular metastases, improving the detection of hypovascular liver lesions in both phantoms and patients (Hokamp et al., 2018). Spectral CT can diagnose diseases based on virtual kV without the need to change the dose compared to the devices available that must be imaged several times to obtain the best diagnosis. Studies performed in previous years examined CNR in the superior mesenteric artery (He et al., 2014, Yin et al., 2017), and hepatic blood vessels (Yin et al., 2018, Zhao et al., 2012).

.

The highest CNR for abdominal angio imaging has been seen in 40 keV monoenergetic images (Doerner et al., 2017b), on a typical CT scan, cholesterol-containing gallstones may seem isoattenuation to the surrounding bile. Studies have shown that virtual monochromatic (VMI) can increase the vision of these stones at both low and high energies, with the greatest improvement (Soesbe et al., 2019), diagnosis of necrotic hepatocellular carcinoma (nHCC) and hepatic abscess (HA) (Yu et al., 2014). In cirrhotic patients, dual-

energy CT enables the prediction of liver-related diseases (Bak et al., 2020, Hong et al., 2022) and the staging of liver fibrosis (Sofue et al., 2018, Lamb et al., 2014).

Also, it can be to differentiate between abscess and metastasis in the liver (Wang et al., 2019), evaluation of the fatty liver (Borges et al., 2023), measure the quantification of iodine in liver lesions (Große Hokamp et al., 2019), and Metastasis assessment in the early stage (Li et al., 2023).

Many attempts have been made to reduce the radiation dose without compromising image quality by using iterative reconstruction (IR) techniques instead of the traditional filtered back projection (FBP) (Singh et al., 2010). FBP is a quick and easy solution that can be obtained from one pass over the acquired data; nevertheless, during acquisition, quantum and electronic noise affect the projection data used in the FBP algorithm. This can occasionally magnify the noise into images, resulting in streaks and other artifacts. As a result, poor noise and image quality are frequently produced when dose reduction is achieved using FBP reconstruction (Hosch et al., 2012).

To get around those restrictions, many IR techniques, including a process known as iterative reconstruction (iDose4) produce lower image noise when compared to the traditional filtered-back-projection (FBP) method (Noël et al., 2011). Iterative model reconstruction (IMR) had a lesser amount of image noise. For diagnosis purposes, the generated IMR image may be utilized in place of traditional FBP images. The goal of IMR is to lower the dosage needed for diagnosis imaging using CT. The therapeutic task, the size of the patient's body, the location of the anatomy, and the clinical setting all influence image quality improvements and dose reduction (Laqmani et al., 2016a).

IMR and iDose algorithms could play an important role in imaging liver disease by reducing the dose of the patient and improving image quality for diagnosis (Kulkarni et al., 2021a, Park et al., 2016).

1.2. Problem statement

The increasing use of CT scans and their associated radiation exposure gives rise to the possibility of radiation-induced cancer. As a result, continual attempts are made to CT radiation doses while maintaining or enhancing image quality, typically with the help of technological innovations in CT scanners and software.

A new imaging device in the West Bank, notably its significant reduction in patient radiation dose. Proper tube voltage adjustment is essential to maintain image quality, as improper settings can increase noise and reduce the signal-to-noise ratio. Advanced imaging processing techniques are also crucial for minimizing noise in CT scans, enabling the reconstruction of high-quality images essential for radiologists in accurately diagnosing liver lesions.

1.3. Aims and objectives

1.3.1. Aims

This study aimed to evaluate the diagnostic accuracy of spectral detector CT 7500 which was recently available at North West Bank to investigate the image quality enhancement based on different virtual tube voltage and reconstruction algorithms to diagnose common liver diseases. In addition, to assess the radiation dose difference between SPCT and MDCT for routine liver CT examinations.

1.3.2. Objectives

1. To assess the best image quality to diagnose different liver diseases using IDOSE with different tube voltages based on virtual tube voltage adjustment

2. To assess the best image quality to diagnose different liver diseases using IMR with different tube voltages based on virtual tube voltage adjustment

3. To compare both algorithms in the diagnosis of common liver pathology in SDCT images

4. To compare radiation dose between SDCT and MDCT.

1.4. Hypotheses of research

The reconstruction algorithms and virtual tube voltage have different abilities to improve liver disease visibility also, there is a significant difference between the Spectral Detector CT 7500 and MDCT for the amount of radiation dose in the diagnosis of liver examination.

1.5. Questions of research

- What is the best reconstruction algorithm for each different liver disease using SPCT?
- What is the tube voltage that is suitable for each liver disease?
- How much is the dose difference between MDCT and SDCT for liver examination?

1.6. Outline

Upon perusing the remainder of this thesis, will encounter the subsequent chapters presented sequentially: -

Chapter (2): Theoretical frameworks and previous Studies

Chapter (3): Material and method of the study.

Chapter (4): The results.

Chapter (5): Discussion and conclusion.

Chapter Two: Theoretical Frameworks and Previous Studies

2.1. Introduction

This study is dedicated to exploring the diagnosis of liver disease by applying spectral CT imaging at the North West Bank. This chapter will present a comprehensive literature review, delve into the theoretical aspects of liver disease, and various types of (SDCT) imaging technologies.

The theoretical framework guiding this research involves an in-depth exploration of key concepts. It will define liver disease, elaborating on its various forms, causes, and prevalence. It will also discuss current methods for diagnosing liver lesions, including traditional imaging techniques and their limitations, to highlight the need for more advanced approaches such as (SDCT) imaging.

This section will focus on the principles and advantages of spectral CT imaging. This method offers unique capabilities for characterizing liver lesions by utilizing different energy levels to improve tissue contrast and enhance detectability.

To ensure a thorough understanding of the landscape of liver disease diagnosis, the literature review conducted for this study is extensive. It explored published studies using databases such as PubMed and Google Scholar, alongside textbook references, to gather relevant information and identify gaps in the current research. This multi-faceted search strategy provides a solid foundation for the subsequent investigation into the effectiveness of (SDCT) imaging in diagnosing liver diseases.

2.2. Theoretical Frameworks

The liver is the largest gland and internal organ in the human body, playing crucial roles in various physiological functions. It is located in the upper right quadrant of the

abdomen, nestled beneath the diaphragm, and located above the stomach and right kidney. The liver's architecture consists primarily of specialized cells known as hepatocytes, which account for more than 80% of the liver's mass. These cells are arranged in functional units called lobules, which contain a network of blood vessels known as sinusoids.

The liver fulfills numerous essential functions that are critical for overall health. One of its primary roles is the metabolism of nutrients. It regulates glycogen storage and release, helping maintain stable blood glucose levels. Additionally, the liver detoxifies various metabolites and drugs, breaking them down and facilitating their elimination from the body. This organ is also responsible for breaking aged or damaged red blood cells, recycling their components to produce vital substances such as hemoglobin.

Another key function of the liver is hormone production. It synthesizes several important proteins, including clotting factors and albumin, which help maintain blood volume and pressure. The liver produces bile, a digestive fluid that emulsifies fats and aids in absorbing fat-soluble vitamins in the intestines.

The liver's vascular system is complex, consisting of the hepatic artery, hepatic vein, and portal vein. The hepatic artery supplies oxygen-rich blood from the aorta, while the portal vein carries nutrient-rich blood from the gastrointestinal tract, spleen, and pancreas to the liver. This dual blood supply is essential for the liver to effectively process nutrients and detoxify harmful substances. The hepatic vein drains deoxygenated blood from the liver and returns it to the heart via the inferior vena cava (Betts et al., 2013).

In terms of anatomical organization, the liver is divided into four main segments: the left lobe, right lobe, caudate lobe, and quadrate lobe. However, according to the couinaud classification system, the liver is more accurately divided into eight functionally distinct

segments, each with its specific vascular input, lymphatic drainage, and outflow. Segment I, known as the caudate lobe, is situated posteriorly and is not visible from the frontal view. Segment IV is sometimes further subdivided into segments IVa and IVb as per the Bismuth classification (Survarachakan et al., 2022).

The separations within the liver are demarcated by major vascular structures, with the middle hepatic vein dividing the left and right lobes. The right hepatic vein further subdivides the right lobe into anterior and posterior sections. The lateral aspect of the left lobe comprises Segments II and III, while Segment IV occupies the medial region, separated by the falciform ligament. The liver itself is anatomically partitioned into upper and lower regions by the portal vein, which is a crucial conduit for nutrient delivery. In summary, the liver's complex structure and diverse functions underscore its importance in maintaining homeostasis and facilitating the body's metabolic activities.

2.2.1 Liver Pathology

The liver can host various types of benign lesions, with four main categories being particularly common. These include hemangiomas, which are vascular tumors composed of a tangle of blood vessels; focal nodular hyperplasias (FNHs), which are benign growths characterized by a hyperplastic nodular formation often stemming from a developmental anomaly; perfusional alterations, which refer to changes in blood flow or perfusion within the liver tissue that may result from various conditions; and liver cysts, which are fluid-filled sacs that can vary in size and are typically benign. Understanding these lesions is crucial for accurate diagnosis and management, as they often present with minimal or no symptoms and can be differentiated from malignant processes through imaging techniques and clinical evaluation.

2.2.1.1 Hepatic Hemangiomas

Hepatic hemangiomas are benign vascular tumors of the liver, found in approximately 20% of the general population, with a higher prevalence in women (Cherqui et al., 1995). Most individuals with hemangiomas are asymptomatic, and these lesions are often discovered incidentally during imaging studies for other conditions. However, in about 40% of cases involving larger giant hemangiomas (those larger than 4 cm), patients may experience symptoms. These atypical symptoms can include nausea, loss of appetite (anorexia), early satiety, and abdominal pain.

Histologically, liver hemangiomas consist of blood-filled vascular sinusoids that are separated by connective tissue septa. Unlike peliosis, these vessels show fibrous trabeculae and an endothelial layer.

Surgical resection of these tumors is generally not recommended due to the very low risk of rupture. However, complications such as sclerosis, calcification, and thrombosis can occur. Hepatic hemangiomas may form concerning factors such as the use of oral contraceptives or during pregnancy, indicating a potential link between hormonal changes and the development of these lesions. Rarely, they can be associated with complicating syndromes like Bornman-Terblanche-Blumgart syndrome, which presents with fever and abdominal pain, or Kasabach-Merritt syndrome, characterized by consumption coagulopathy.

These tumors are believed to arise spontaneously with no well-established causes; some theories suggest a genetic basis or hamartomas. Alternatively, they may arise from the enlargement of pre-existing blood vessels during normal tissue development (Shaked et al., 2011). The observed growth patterns of these lesions suggest ongoing vascular dynamics. Autopsy studies have revealed a prevalence range of 0.4–20%, positioning hepatic

hemangiomas among the most common benign liver lesions encountered (Craig et al., 1989).

2.2.1.2 Focal Nodular Hyperplasia (FNH)

Focal nodular hyperplasia is recognized as the second most prevalent benign hepatic lesion after hemangiomas, accounting for about 8% of initial hepatic lesions (Craig et al., 1989). It predominantly occurs in women at a ratio significantly higher than that of men, with an estimated frequency of 0.9%. Most cases of FNH are asymptomatic and discovered incidentally. Hemorrhage and rupture of FNH lesions are uncommon, and there is no associated risk of malignancy (LeGout et al., 2022).

FNH lesions are hypothesized to develop from hyperplastic bile ducts that lack proper connection to the biliary tree since certain theories propose that they are congenitally excluded (Ammori et al., 2002). Structurally, they are characterized by an outer fibrous capsule lined by cuboidal to columnar epithelial cells that actively secrete cystic fluids (Sanfelippo et al., 1974). FNH is most frequently observed in women aged 20 to 50, with an incidence rate of approximately 80%. The pathophysiology remains uncertain but may involve vascular damage.

Lesions are typically less than 3 cm in diameter, asymptomatic, and most often incidentally identified during imaging. The differentiation of FNH from other conditions such as adenomas or fibrolamellar carcinomas presents a significant diagnostic challenge. Notably, fibrolamellar carcinomas frequently show enlarged lymph nodes, central calcifications, washout phenomena, and heterogeneous enhancement—all features not commonly found in FNH. Clinically, FNH is characterized by the absence of symptoms, normal liver function tests, and a non-history of oral contraceptive use (Lizardi-Cervera et al., 2006).

2.2.1.3 Hepatic Adenoma (HA)

Hepatic adenomas are primarily observed in individuals with diabetes or in women who have used oral contraceptives for extended periods, typically more than five years. The development of multiple adenomas has been correlated with glycogen storage diseases, specifically types I and III. In particular circumstances such as anabolic or androgenic steroid use, patients may develop adenomatosis, characterized by the presence of more than ten adenomas. Patients frequently report abdominal discomfort, which can be a significant symptom (Erdogan et al., 2006).

Adenomas typically appear as either hypo- or hyper-echoic lesions on ultrasound and hypo- or hyper-dense on CT imaging, revealing substantial variability in their imaging characteristics. MRI may not provide precise differentiation in some cases. Lesions are usually less than 8 cm in size, but larger adenomas measuring more than 15 cm may occur, revealing a histological pattern of monotonous sheets of small or normal hepatocytes without central veins, portal tracts, or bile ducts. It is noteworthy that hepatocellular carcinoma (HCC) can develop in about 5% of patients with hepatic adenomas (Colli et al., 2007).

Spontaneous rupture and subsequent hemoperitoneum are relatively rare but represent about 10% of cases and are often linked to triggers such as menstruation, pregnancy, or the postpartum state. Most hepatologists advise discontinuation of oral contraceptives and consider surgical resection for symptomatic patients (Demarco et al., 2006).

2.2.1.4 Partial Nodular Transformation (PNT)

Partial nodular transformation is associated with a variety of medical conditions, including Behcet's disease, rheumatic disorders, myeloproliferative disorders, chronic venous congestion, metastatic neuroendocrine tumors, and Budd-Chiari syndrome. Certain medications, such as steroids, contraceptives, antineoplastics, and immunosuppressants, have also been implicated in these cases. PNT may lead to cholestasis and portal hypertension in some lesions, which complicates the clinical picture. Open liver biopsy is rarely required for diagnosis (Trenschel et al., 2000). The development of PNT may also occur as a result of compensatory hyperplasia and parenchymal atrophy secondary to portal vein thrombosis, further collaborating on the complex pathophysiology underlying this condition.

2.2.1.5 Hepatobiliary Cyst Adenoma

This rare form of tumor primarily affects middle-aged women and is characterized by abdominal pain. Differing from benign hepatic cysts, hepatobiliary cyst adenomas possess a thick, septate membrane. Given that up to 25% of these lesions can undergo malignant transformation into cystadenocarcinomas, surgical excision is typically recommended as a precautionary approach (Wheeler and Edmondson, 1985).

2.2.1.6 Bile Duct Adenoma (Cholangioma)

A benign biliary tumor, bile duct adenoma is composed of very small bile ducts that are evenly spaced against a fibrotic stroma background. Bile duct adenomas also referred to as cholangiomas, are associated with conditions like α-1-antitrypsin deficiency. These tumors present as solitary subcapsular nodules, measuring between 1 to 20 mm, and are characterized by a lack of bile in the small bile ducts. This pathology rarely and cannot be differentiated from intrahepatic cholangiocarcinoma. The diagnosis is confirmed by immunohistochemical histology and surgical removal (Teng et al., 2022).

2.2.1.7 Mesenchymal Hepatic Hamartoma

After infantile hemangioma, hepatic mesenchymal hamartoma (HMH) is the second most prevalent benign liver tumor in infants. 80% of instances happen within the lesion, which accounts for 8% of all pediatric liver tumors. the initial two years of existence. There have also been reports of HMH cases in adults and pregnant women. HMH exhibits a little male predominance in the pediatric series. In contrast, females are more likely to exhibit adult HMH. Abdominal distention and/or upper abdominal mass are common presentations for patients with HMH. In children, the right lobe of the liver is more commonly affected, while in adults, both lobes are similarly damaged (Martins-Filho and Putra, 2020).

2.2.1.8 Pseudo-lesions

Pseudo-lesions refer to non-diseased abnormalities of the liver that can mimic or hide actual liver lesions known as hepatic pseudo lesions. Because of the liver's distinct dual blood supply and the multilayer anastomosis that exists between them, it is more prevalent there. Areas that may mimic lesions radiologically but do not represent genuine pathological changes. These can present diagnostic challenges in clinical practice, necessitating careful interpretation of imaging findings to avoid misdiagnosis (Li et al., 2022).

2.2.1.9 Polycystic Liver Disease (PCLD)

Polycystic liver disease (PCLD) is classified within the broader medical category of ciliopathies, which are disorders stemming from dysfunction in cilia, the small hair-like structures on the surface of cells. PCLD encompasses a range of conditions, including micro hamartomas, choledochal fibroid cysts, congenital hepatic fibrosis, and Caroli's disease. These conditions are primarily associated with genetic mutations that impair the normal

function of cholangiocyte ciliary processes, which are essential for maintaining biliary and hepatic function.

A hallmark of PCLD is the presence of extensive hepatic cysts that differ from simple hepatic cysts in both size and quantity. Typically, patients with PCLD develop more than 20 cysts, which are larger and can significantly distort liver architecture. These cysts are often classified as microscopic but exhibit a characteristic morphology and distribution throughout the liver (Drenth et al., 2010).

In addition to the cysts, PCLD is also associated with specific perfusional changes in the liver. Areas of fatty sparing can be observed, which demonstrate unique patterns and enhanced imaging features. These changes are so distinctive that they often allow for a definitive diagnosis to be made based on imaging studies alone, minimizing the need for additional diagnostic investigations (Jang et al., 2017).

2.2.1.10 Fatty Liver

Nonalcoholic fatty liver disease (NAFLD) encompasses a spectrum of liver disorders characterized by the accumulation of fat within liver cells, or steatosis, without a significant history of alcohol consumption. This condition is increasingly prevalent among individuals with obesity-related metabolic disorders, such as type 2 diabetes, dyslipidemia (abnormal lipid levels), and metabolic syndrome. Interestingly, NAFLD is not restricted to those who are obese; it can also manifest in individuals who are of normal weight.

 Studies have shown that even among non-obese populations, which include children and adults across diverse ethnic backgrounds, cases of NAFLD have been documented. Notably, research indicates that individuals of Asian descent may have a higher prevalence

of NAFLD compared to other ethnic groups, reflecting potential genetic and environmental influences (Kim and Kim, 2017).

The distribution of fat in the liver is not uniform. In approximately 10% of cases, fat may accumulate in specific areas, with the anteromedial section of the left lobe often being affected. Patients who present with fatty liver disease frequently have comorbid conditions such as steroid use, alcohol consumption, diabetes mellitus, hyperlipidemia, and obesity, which can exacerbate the condition.

In diagnostic imaging, fatty liver appears hyper-echoic on ultrasound, indicating an increased reflectivity due to fat deposits. Furthermore, CT scans reveal that fatty liver has low attenuation, which means it does not absorb X-rays effectively, allowing for differences in tissue density to be perceived. Importantly, focal areas of fatty liver typically do not displace intrahepatic blood vessels, a finding that is crucial for differentiating between simple steatosis and other liver pathologies (Perlemuter et al., 2007).

Understanding these nuances of NAFLD is essential for proper diagnosis and management, particularly considering the increasing incidence of this condition in various populations.

2.2.1.11 Hepatocellular Carcinoma (HCC)

The most prevalent form of liver cancer, accounting for approximately 75% of all liver cancer cases (McGlynn et al., 2021). This malignancy primarily arises from hepatocytes, the main liver cells, and is often associated with underlying liver conditions such as cirrhosis, hepatitis B, and hepatitis C infections.

Clinically, patients with HCC may experience a range of symptoms, the most common of which include persistent pain in the right upper quadrant of the abdomen and unintentional weight loss. As the disease progresses, additional signs may emerge, such as jaundice (yellowing of the skin and eyes), ascites (fluid accumulation in the abdomen), and general fatigue.

A critical aspect of HCC is its association with cirrhosis. In patients who already have cirrhosis, the worsening functionality of the liver may raise suspicion for HCC, particularly when accompanied by such clinical features. Additionally, HCC can lead to acute complications, such as a severe abdominal crisis resulting from a ruptured liver tumor, which can cause significant intra-abdominal hemorrhage, necessitating immediate medical intervention.

Interestingly, there is a growing trend towards the identification of asymptomatic HCC. Many patients are diagnosed during evaluations for liver transplantation or while undergoing routine screening procedures, such as imaging studies, particularly in individuals with cirrhosis. This highlights the importance of regular monitoring in high-risk populations to facilitate early detection and potentially improve outcomes(Befeler and Di Bisceglie, 2002).

2.2.1.12 Metastatic Cancer

Metastatic cancer refers to the process when cancer cells spread from their primary site to other areas of the body. One of the most common sites for metastasis is the liver, particularly from cancers of the gastrointestinal system, including the pancreas, breast, and lung. Colorectal cancer is the leading cause of liver metastases. When imaging the liver for potential metastases, several abnormalities may suggest the presence of cancer. Notably,

solitary lesions are observed in only about 20% of liver metastases, indicating that multiple lesions or extensive liver involvement are more common (Tsilimigras et al., 2021).

Both lobes of the liver are typically affected in cases of metastasis. In particular, colorectal metastases are identifiable on CT scans as poorly defined lesions with low attenuation; these lesions often exhibit necrotic centers and irregular, uneven edges.

When performing dynamic CT imaging, these metastatic lesions tend to demonstrate increased visibility during the early vascular phase, providing crucial information for diagnosis. Additionally, incorporating CT arterial portography into the imaging process significantly enhances sensitivity, achieving approximately an 85% accuracy rate in detecting metastases. Furthermore, intraoperative ultrasound (US) is recognized for its exceptional sensitivity and specificity when evaluating colorectal cancer metastases during surgical procedures.

The term "metastasis" is used when cancerous cells spread from their original tumor site to distant locations in the body. The liver is frequently a common site of metastasis, particularly from tumors originating in the colon. Notably, over half of the patients diagnosed with colorectal cancer will eventually develop liver metastases, which poses significant challenges for treatment and management.

In pediatric cases, hepatoblastoma stands out as the most prevalent malignant liver tumor that affects infants and young children, with the majority of cases diagnosed in the first two years of life (Sharma et al., 2017). In adolescents and adults, the most common primary malignancy affecting the bile ducts is known as cholangiocarcinoma (CCA). CCA accounts for 10%–15% of hepatobiliary tumors, and its incidence has been on the rise over recent years. The malignant transformation responsible for CCA occurs in cholangiocytes,

the specialized epithelial cells that line the biliary system and regulate bile flow (Lazaridis and Gores, 2005).

2.2.1.13 Fibrolamellar Malignancy

Fibrolamellar carcinoma is recognized as a distinct subtype of hepatocellular carcinoma (HCC) that diverges significantly from traditional HCC risk factors, such as chronic viral hepatitis or cirrhosis. Unlike more common forms of liver cancer, fibrolamellar malignancy typically arises in younger individuals, with an average onset age of around 26 years.

Clinically, this condition often presents as a large, painful mass predominantly located in the left lobe of the liver. Patients may experience abdominal discomfort or pain as the tumor grows. Histologically, fibrolamellar carcinoma is characterized by its unique "fibrolamellar" pattern. This pattern is marked by the presence of thin layers of fibrosis that partition the neoplastic hepatocytes, creating a distinctive appearance under a microscope. This structural feature is integral to the diagnosis of the malignancy. At the time of diagnosis, approximately 50% of fibrolamellar lesions are amenable to surgical resection. This high rate of resectability is crucial, as surgical removal of the tumor remains the most effective treatment option and can lead to better patient outcomes compared to non-surgical approaches (Abdelhamed and El-Kassas, 2022).

2.2.15.14 Intrahepatic Cholangiocarcinoma (iCCA)

Is recognized as the second most common type of primary liver cancer, following hepatocellular carcinoma. In the United States, the incidence of primary liver cancer is estimated to impact around 40,000 individuals each year. Of these cases, iCCA accounts for

approximately 15% to 20%, translating to roughly 6,000 to 8,000 new cases annually. The mortality rate associated with iCCA is notably high, with the cancer responsible for around 20% of all liver cancer-related deaths (McMillan et al., 2022).

Over the past several decades, particularly since 1973, there has been a concerning trend in both the incidence and mortality rates of iCCA, with an increase occurring approximately every ten years. This rise can be attributed to factors such as aging populations and potential environmental factors, but the precise reasons remain an area of active research.

To diagnose liver diseases should do multiple examinations including laboratory and radiology examinations. Surgical resection is currently regarded as the only well-established curative treatment option for iCCA. Unfortunately, surgery is not feasible for a significant number of patients, primarily because their cancer is diagnosed at a more advanced stage or because they already present with underlying liver disease, such as cirrhosis or hepatitis. Consequently, these patients may require alternative therapeutic approaches, including chemotherapy, targeted therapy, or palliative care, to manage their condition and improve their quality of life.

2.2.1.15 Epithelioid Angioendothelioma (EHE)

Epithelioid angioendothelioma (EHE) is a rare form of vascular endothelial cell neoplasm characterized by the presence of epithelioid cells and histiocyte-like cells embedded within a mucus or fibrotic stroma. The World Health Organization (WHO) classifies EHE as a tumor that possesses full malignant potential, indicating its capacity for aggressive behavior and metastasis.

EHE can manifest in various anatomical locations throughout the body, impacting areas such as the lungs, soft tissues, head and neck regions, pleura, bones, and other organs.

The hepatic variant, known as hepatic EHE (HEHE), is particularly rare, with an incidence estimated at one to two cases per million people. This liver-affecting subtype predominantly affects women, with the highest incidence occurring in individuals aged 30 to 50 years, reflected in a male-to-female ratio of approximately 2:3 (Kou et al., 2020).

Histologically, HEHE can be categorized into several forms: diffuse, multifocal, and solitary lesions, with the multifocal variant being the most frequently observed. The malignancy of HEHE is described as intermediate, situated between that of a benign hemangioma and a more aggressive hemangiosarcoma of the liver. These tumors typically display a low to medium grade of malignancy, suggesting that while they can be aggressive, they may also exhibit variable behavior (Kou et al., 2020).

Upon examination, HEHE reveals a composition of dendritic-like cells alongside atypical epithelioid tumor cells, which demonstrate invasive properties, particularly in the hepatic sinusoids, leading to significant disruption of normal liver architecture. In advanced stages, focal complications may arise, often associated with the infiltration of adjacent structures such as the portal vein and hepatic vascular system. This advancing stage generally presents with a diffuse radiological appearance and is commonly linked to distant metastases, complicating the clinical management of patients (Kou et al., 2020).

Extrahepatic involvement frequently occurs, with the lungs, peritoneum, spleen, lymph nodes, and bones identified as the most common sites of metastasis, indicating the aggressive and multifaceted nature of this neoplasm (Kou et al., 2020). Understanding the behavior and characteristics of EHE, particularly its hepatic variant, remains critical for developing effective treatment strategies and improving patient prognoses.

2.2.1.16 Leukemias and Lymphomas

Can significantly affect the liver, particularly in the context of Hodgkin's disease. This form of cancer often leads to liver involvement through various mechanisms, including the development of sepsis, complications introduced by medications, and viral hepatitis that may accompany the disease. Additionally, infiltration of the liver by lymphoma manifests as either numerous tiny nodules or larger, palpable masses.

One notable condition associated with Hodgkin's disease is vanishing bile duct syndrome, although instances of cholestasis are rare in this context. In evaluating liver involvement, it is essential to consider a differential diagnosis that includes T-cell lymphomas, as well as lymphomas characterized by reactive infiltrate, which may present similarly.

In more uncommon scenarios, primary hepatic lymphoma can arise, presenting as hepatic failure. This can occur alongside elevated lactate dehydrogenase (LDH) levels, reflecting the extent of liver involvement. Patients may exhibit diffuse hepatic involvement characterized by hepatomegaly or may present with one or multiple distinct hepatic masses.

Furthermore, there have been documented cases of peripheral gamma delta T cell lymphomas that not only affect the liver but also involve the spleen, leading to significant hepatic sinusoidal infiltration. Other hematological conditions, such as multiple myelomas or various forms of leukemia—including chronic lymphocytic leukemia and hairy cell leukemia—can also infiltrate life (Thandra et al., 2021). This infiltration can occur either in a localized manner or diffuse throughout the liver, complicating the clinical picture and necessitating a thorough diagnostic approach.

2.2.1.17 Focal Liver Lesion Differential Diagnosis

The initial and critical step in the characterization of a localized hepatic lesion observed on a CT scan involves assessing its density. When evaluating a lesion, the presence of near-water density, combined with a homogeneous internal structure and well-defined, sharp margins, suggests the possibility of a cyst. To confirm this diagnosis, additional imaging modalities such as US, equilibrium-phase CT scanning or magnetic resonance imaging (MRI) can be employed. In particular, MRI, with its T2-weighted sequences appearing bright and the absence of enhancement post-gadolinium administration, is particularly effective in ruling out solid components or lesions along the mural wall.

Radiologists must also be aware of the imaging features of other cystic lesions that may mimic simple cysts, as differential diagnosis is crucial. When analyzing solid hepatic lesions, observing the degree and pattern of contrast enhancement becomes essential for accurate disease characterization. For example, a hemangioma is typically indicated by a characteristic pattern of peripheral and nodular enhancement, with the density of these enhancing regions maintaining consistency across the arterial, venous, and delayed phases of imaging.

In more complex cases, primary hepatic lymphoma, though rare, can present in various ways. It may cause hepatic failure alongside marked elevation of lactate dehydrogenase (LDH), manifest as diffuse hepatic infiltration resulting in hepatomegaly, or as single or multiple distinct masses. Notably, certain reports have documented the presence of peripheral gamma delta T cell lymphomas showing involvement of the spleen and significant infiltration of the hepatic sinusoids.

Another aspect to consider is the infiltration of the liver by conditions such as multiple myeloma or leukemias (including chronic lymphocytic leukemia and hairy cell leukemia),

which can affect the liver either locally or diffusely. Furthermore, several arterially hypervascular lesions warrant consideration, including FNH, HCA, HCC, and metastases originating from neuroendocrine tumors, melanoma, renal cell carcinoma, and breast cancer. Notably, HCC is frequently evaluated in the context of underlying chronic liver disease or cirrhosis, which can influence imaging findings.

In clinical practice, young women without pre-existing cirrhosis who exhibit homogeneous, nearly isodense or isointense lesions on unenhanced CT or MRI, particularly when associated with a central hyperintense scar seen on T2-weighted imaging, may be more likely to present with FNH. Conversely, the presence of a malignant mass, such as metastases or HCC, is suggested when imaging reveals thick, irregular, and heterogeneous enhancement patterns or the occurrence of peripheral washout during the delayed phase.

2.2.1.18 Cholangiocarcinoma (CC)

Is specifically characterized by its delayed enhancement, which is attributed to its fibrotic stroma (Schima et al., 2018). Understanding these nuanced differences in imaging characteristics is vital for accurate diagnosis and subsequent management of focal liver lesions.

2.2.2. Diagnostic Imaging of Liver Diseases

Diagnostic imaging plays a crucial role in identifying and characterizing liver diseases, leveraging various imaging modalities to provide accurate and noninvasive assessments of hepatic focal lesions. A careful examination, paired with an understanding of the unique features associated with each imaging technique, can lead to an effective diagnosis in the appropriate clinical context.

The primary imaging modalities utilized in the evaluation of liver diseases include magnetic resonance imaging (MRI), computed tomography (CT), and hepatic ultrasonography (US). Each of these techniques offers distinct advantages and can visualize different aspects of liver pathology (Azizaddini and Mani, 2020).

2.2.4 Ultrasound (US)

Ultrasound, or ultrasonography, is a widely utilized imaging technique for the initial assessment of abdominal conditions. This method is particularly advantageous due to its cost-effectiveness, accessibility, and non-invasive nature, making it an ideal choice for many patients. Additionally, ultrasound does not expose patients to ionizing radiation, which is a significant consideration in medical imaging.

For patients with a history of liver cirrhosis or viral hepatitis, it is recommended that they undergo semi-annual ultrasound scans. These regular screenings are crucial for the early detection of liver abnormalities, allowing for timely intervention and management. Moreover, ultrasonography is frequently performed on patients presenting with symptoms such as abdominal pain or elevated liver function tests, which may indicate underlying hepatic issues. Interestingly, liver abnormalities are often discovered incidentally during ultrasonography conducted for unrelated medical reasons. This serendipitous finding underscores the importance of ultrasound in routine imaging practices.

However, one notable limitation of ultrasound in the evaluation of focal liver lesions is the potential difficulty in achieving a definitive diagnosis. The images obtained from ultrasound can sometimes be inconclusive, necessitating further diagnostic investigations. In such cases, additional imaging modalities, such as CT or MRI, may be required to

provide a clearer picture. Occasionally, a liver biopsy may also be necessary to ascertain the nature of a particular lesion definitively (Xi et al., 2021).

Ultrasound is particularly adept at evaluating vascular flow within the liver, making it a valuable tool for detecting gallbladder pathology or biliary obstructions. It excels in differentiating between cystic and solid liver lesions, providing clinicians with important information about potential hepatic conditions. Nonetheless, it is essential to note that while ultrasound is effective in many scenarios, it is not as sensitive as MRI or CT in detecting certain liver abnormalities. Thus, it is often used as a preliminary screening tool, with more advanced imaging techniques employed as needed for comprehensive assessment (Glover et al., 2002).

2.2.5 Magnetic Resonance Imaging (MRI)

Magnetic Resonance Imaging (MRI) stands out for its exceptional spatial and contrast resolution, which significantly enhances diagnostic accuracy and detail in comparison to CT. One of its most notable advantages is the absence of ionizing radiation, making it a safe option for patients who require multiple imaging studies. Additionally, the contrast agents used in MRI are generally safe for individuals with renal insufficiency, a demographic that poses challenges for CT contrast agents.

Another critical benefit of MRI lies in its utility for patients who have experienced allergic reactions to iodinated contrast media. In these cases, unenhanced MRI can often provide superior diagnostic capabilities as compared to unenhanced CT, thereby offering a viable alternative for these patients. However, it is essential to note that while MRI can be utilized safely, certain limitations condition its use, primarily related to patient comfort and convenience. Key drawbacks of MRI include its typically higher cost and the longer duration required for imaging procedures. Furthermore, patients often face the challenge of

needing to hold their breath for extended periods during scans, which can be uncomfortable or difficult for some individuals (Kamel and Bluemke, 2003).

In clinical practice, MRI serves as a complementary diagnostic modality to CT, particularly noted for its enhanced ability to characterize small lesions, such as those measuring 3 cm or less. Despite its advantages, MRI is not typically employed as a first-line imaging modality; the intricate protocols and extended acquisition times hinder its use in routine diagnostics. Notably, there has been a measurable increase in MRI acquisitions across Europe, with a 14.48% rise per 1,000 individuals reported from 2013 to 2018.

An MRI should be done to diagnose invisible metastases. MRI makes it possible to differentiate primary liver tumors from treatment-related liver alterations in melanoma, colorectal cancer, and neuroendocrine tumor metastases. Hypersteatosis, focal fat, and nodules that resemble focal nodular hyperplasia in patients treated with platinum-based chemotherapy can all appear to be metastases. When a cancer patient has a fatty liver, an MRI is better than a CT. MRI can be utilized as a problem-solving technique, even if CT is the first-line imaging for metastases. For patients undergoing metastatic surgery or curative surgery, MRI may be the first-line procedure (Karaosmanoglu et al., 2016).

When interpreting MRI images, particularly T2-weighted imaging, differentiating lesions from surrounding parenchyma can be challenging. The lesion tissue frequently appears hyperintense or isointense relative to the adjacent healthy tissue, but T2-weighted images may sometimes yield isointense findings that are insufficient for a precise characterization of liver lesions. Conversely, when employing T1-weighted imaging, liver lesion tissue typically presents as hypointense, providing clearer differentiation. However, it is crucial to acknowledge that lesions measuring less than 1.5 cm may often appear isointense on T1-weighted images, which could complicate the diagnosis (Survarachakan et al., 2022).

2.2.6 Computed Tomography (CT)

CT represents one of the most transformative advancements in medical imaging, offering detailed anatomical insights that are especially effective in differentiating soft tissue structures. This form of imaging enables a level of diagnostic precision that is unparalleled when compared to traditional imaging techniques. By integrating two-dimensional images and cross-sectional views, a three-dimensional representation of the scanned area can be constructed, significantly enhancing the clinician's ability to analyze and interpret complex anatomical relationships.

For the majority of cancers that start outside of the central nervous system, multidetector-row computed tomography (MDCT) is now recognized as the best imaging test for staging and monitoring. The detection of liver metastases has been improved as a result of technological advancements in this imaging approach. The finding of incidental hepatic lesions in cancer patients that were previously undiagnosed is an unexpected consequence of this increased diagnostic acumen. These common, unintentionally discovered liver lesions have presented radiologists and doctors with a therapeutic conundrum (Gore et al., 2012).

Since the early 1980s, when more than three million CT scans had already been performed (Bercovich and Javitt, 2018), the field of CT imaging has experienced explosive growth. Reports show that over 100 million CT scans are now conducted annually (Kontis et al., 2017), highlighting the essential role that CT plays in modern medical diagnostics. This rise can be attributed to numerous technological advancements in CT systems, which include faster scanning processes, thinner image slices, reduced radiation exposure, and higher-quality output.

In stark contrast to the standard practice of twenty-five years ago, where a typical CT study could take several minutes to complete depending on the specific machine and scanned volume, contemporary CT investigations can often be finished in mere seconds. Modern scanners can cover extensive anatomical regions rapidly, sometimes utilizing

multiple energy levels during a single examination, all while producing slices as thin as just a few millimeters (Wilk, 1959). Furthermore, significant advancements in image reconstruction methodologies and the introduction of more efficient, larger detector materials have resulted in a dramatic reduction of radiation doses by as much as 50%, while concurrently improving image quality (Willemink et al., 2014).

Intravenous contrast agents significantly enhance the diagnostic utility of imaging studies by facilitating the differentiation of lesions based on their composition, vascularity, and perfusion characteristics. In liver imaging, there are generally three critical phases to consider following the administration of contrast. Arterial Phase, this phase captures early vascularization of lesions, which is essential for identifying hypervascular tumors such as hepatocellular carcinoma.

The arterial phase, redistribution or portal venous phase, and equilibrium or hepatic venous phase are the three idealized perfusion phases that comprise the entire hepatic perfusion cycle. To achieve uniform flow rates of 2.5–5 mL/sec, the contrast agent and saline "chaser" should be applied using mechanical power injectors using 16–20 gauge indwelling venous catheters. An overall contrast agent volume of up to 80 mL is enough to perfuse the liver with 30 g of iodine when nonionic and more highly concentrated contrast agent solutions with an iodine concentration of 370 mg/mL are used in adults.

This results in a significant increase in iodine application during the arterial phase while significantly lowering the total injected iodine dose when compared to less concentrated contrast agent solutions. Lastly, it is advised to employ the bolus monitoring methods provided by all multidetector CT systems to ascertain the arrival timing of the contrast agent bolus to account for the individual variances of cardiac output, blood volume, and visceral perfusion. Bolus tracking depends on obtaining successive low-dose images of parenchymal or vascular structures. evaluation of the associated enhancement values and the start of the scanning procedure following the achievement of a predetermined attenuation threshold (Boll and Merkle, 2009).

Portal Venous Phase, this phase follows the arterial phase and allows for a more detailed evaluation of the liver parenchyma and lesions about the portal venous supply, which is particularly useful for categorizing tumors and assessing hepatic perfusion. Delayed Phase, in this phase, imaging is acquired at a later time point, which can help illustrate the washout characteristics of lesions, further aiding in the differentiation of benign and malignant conditions.

The patterns of extracellular parenchymal contrast material uptake and the corresponding variations in tissue attenuation over time follow a complex multicompartmental model due to this dual-source hepatic blood supply.

For the majority of hepatic lesions, contrast-enhanced multidetector computed tomography (MDCT) is considered the preferred modality due to its high resolution and speed, making it effective for detecting and accurately characterizing liver abnormalities. However, hepatic ultrasonography serves as an invaluable screening tool, particularly in initial assessments, due to its accessibility, safety, and cost-effectiveness (Azizaddini and Mani, 2020).

2.2.3 CT generations

The "translate–rotate" concept served as the foundation for the first generation of CT systems, which began with Sir Godfrey Hounsfield's initial head scanner (Ambrose, 1973). second-generation CT systems: however, an array of around 30 detectors that covered a fan angle of roughly 10 took the place of the single detector. Consequently, a slice's acquisition time may be lowered to 18 seconds.

Single-slice CT scanners were used in the second generation. Prior to the recent recovery of "multi-slice" scanning in the mid-1990s, most scanner designs did not have multiple detectors in the through-plane direction, as was already the case with the first generation of CT scanners. Third-generation scanners are currently the most widely used

CT equipment. They use a technique known as "rotate rotate" geometry, in which a detector array and an X-ray tube both revolve around the patient. Regular body scanning became possible since the detector's fan angle is sufficiently wide (about 45–55) to cover a wholebody SFOV with a diameter of 50 cm.

The measurement system could therefore rotate continuously thanks to slip-ring designs that routed electrical impulses over sliding contacts. This removed the need to rewind the gantry after each turn to prevent cable tangling. The most rapid CT scanner available in 2012 required 0.27 seconds for the tube and detector system to rotate 360 degrees.

Additionally, spiral (helical) CT scanning with continuous data gathering and continuous table movement—which has transformed medical CT since 1990—required slipring gantries (Kalender et al., 1990). Spiral CT allows for the examination of whole organs, including the liver and lungs, in a single breath held without the risk of anatomical information being mis- or double-registered. The fourth generation has a stationary array of detectors surrounding the patient in addition to a revolving X-ray tube and a broad fan beam. Signal data did not need to be passed over the moving gantry in these systems, which had fewer moving parts.

They could allow the X-ray tube to rotate around the patient very quickly, meaning that each slice would only need very brief acquisition times. However, due to the high system costs resulting from the numerous detector elements and other issues, the design idea has currently been abandoned. For instance, the images suffered from severe scatter artifacts and it was not possible to utilize targeted post-patient collimators (near the detector surface) to suppress dispersed radiation (Flohr, 2013).

MDCT the third-generation rotate-rotate geometry-based MDCT devices have controlled the CT field since the late 1990s. X-ray detectors that are physically separated in the z-axis direction and allow for the simultaneous capture of several slices of the patient's

anatomy are the most significant advancement in these CT scanners. Faster scan speeds, better through-plane resolution, and more efficient use of the available X-ray tube power are some of the main advantages of MDCT systems. Additionally, MDCT entered new therapeutic domains, including coronary artery CT angiography with ECG gating capacity.

Detectors having more detector rows than the final read-out slices are utilized to provide slices at various collimated slice widths. Pre-patient collimation modifies the overall beam width in the z-direction, and the signals from each of the two or more detectors along the z-axis are electronically merged to create thicker slices. The first MDCT systems introduced in 1998 offered the simultaneous acquisition of four slices with the thinnest collimated slice width of 1 or 1.25 mm at a rotation time of down to 0.5 s (KlingenbeckRegn et al., 1999). Although an 8-slice CT system (thinnest collimation 8 9 1.25 mm) was released in 2000, it did not increase the spatial resolution but allowed for shorter examination periods.

Siemens aimed to reduce spiral artifacts and boost through-plane resolution without pitch by concurrently acquiring 64 overlapping 0.6-mm slices with a total z-coverage of 19.2 mm using 32 physical detector rows and a z-flying focus spot (Flohr et al., 2005). It became possible to perform CT scans with isotropic sub-mm resolution, even over broad anatomical ranges, thanks to 64-slice CT equipment. One vendor presented an MDCT device with 128 concurrently acquired slices in 2007.

It was built around a 64-row detector with a z-flying focus spot and 0.6-mm collimated slice width. It is now possible to acquire 256 slices at once using a CT system that has a z-flying focus spot and a 128-row detector (0.625-mm collimated slice width). According to clinical experience with 64-, 128-, or 256-slice CT, MDCT performance has reached a saturation point, and just adding additional detector rows won't result in more therapeutic benefit. Rather, efforts to address the remaining MDCT restrictions are still in progress.

More expansive detectors with a max of 320 detector rows covering 16 cm along the z-axis and quick gantry rotations of less than 0.25 seconds are features of luxury CT scanners (Lell and Kachelrieß, 2020). In comparison to the one-shot arterial phase, wide-detector CT scanners enable protocols that scan the entire liver (in axial view) at numerous time intervals throughout the early-late vascular phase, which could detect additional hypervascular lesions within the liver (Soloff et al., 2020).

Multidetector row CT, commonly referred to as MDCT, employs an array of multiple parallel rows of X-ray detectors. These scanners are typically available in configurations with 4, 8, 16, 64, 128, 256, 340, or even 640 detector rows, depending on the specific device. During each rotation of the gantry, each detector row captures its set of data, thereby allowing for a much larger volume of the patient to be scanned with each complete revolution. The effectiveness of MDCT is also influenced by pitch, which is determined by the ratio of the table travel during a full gantry rotation to the total width of all the active detectors.

Notably, the widths of the narrowest detector rows can vary across different scanners and manufacturers, typically ranging from 0.5 to 1 mm. For example, 16-row detectors collectively provide coverage of about 20 mm, while 64-row scanners can achieve approximately 40 mm of coverage (Webb, 2006).

In the last twenty years, the evolution of MDCT has supported three major imaging trends: an increase in the number of slices obtained, greater speed in acquisition times, and a significant reduction in radiation doses. One of the crucial factors driving the advancement of multislice CT technology has been the development of solid-state detectors, which are organized into arrays of detector elements. This innovation allows for more extensive coverage in each rotation of the scanner (Shefer et al., 2013).

Additionally, CT x-ray sources have been engineered to enable higher acceleration and deliver greater peak power, facilitating quicker scanning without compromising image

quality. Meanwhile, advances in detection systems have shortened integration times, thus facilitating faster acquisition speeds. Recently, the emergence of iterative reconstruction techniques has further optimized these systems, encouraging the use of low and ultra-low radiation dose scanning protocols.

2.2.7 CT Innovation

The exploration of dual-energy computed tomography (CT) techniques began in 1976 when researchers Alvarez and Macovski conducted foundational studies that demonstrated the viability of differentiating between the contributions of the photoelectric effect and Compton scattering mechanisms in the measured attenuation coefficients of tissues (Alvarez and Macovski, 1976). This groundbreaking research revealed that even when utilizing combined X-ray spectra, it was possible to analyze and separate the distinct interactions of X-rays with various materials based on their energy levels.

Since that pivotal study, the field has advanced considerably with the development of various technical methodologies to acquire dual-energy data sets. One noteworthy approach that has emerged involves a modified scanning strategy. In this method, one axial scan—consisting of a single rotation of the X-ray tube—is performed at each predetermined tube potential before the table is incremented. This innovative technique aims to mitigate the time delays that are typically associated with executing two consecutive scans across the full anatomical region of interest. By shortening the temporal gap between the acquisition of lowenergy and high-energy images, this strategy significantly enhances the overall scanning efficiency.

Additionally, the use of partial scan reconstruction techniques has been optimized to achieve the highest temporal resolution possible. This process involves capturing 180 degrees of projection data alongside the fan angle for each tube potential, with a brief pause inserted between acquisitions. This brief pause allows time for changing the tube potential and for the table to move, which minimizes any motion artifacts and improves image clarity.

Such a method is particularly beneficial for imaging organs or tissues that remain largely static, making it an appropriate choice for certain clinical scenarios where precision and speed are crucial (McCollough et al., 2015).

2.2.8 Spectral Computed Tomography

Spectral computed tomography (CT) has emerged as a significant advancement in medical imaging, offering enhanced diagnostics through the analysis of different energy levels of X-ray beams. There are two primary types of clinical CT scanners available for spectral CT acquisition: detector-based scanners and source-based scanners.

2.2.8.1 Source-Based Scanners

These scanners utilize X-ray beams that emit a range of energy spectrums, allowing for the differentiation of materials based on their atomic composition and density. Sourcebased scanners can achieve this by employing either a single X-ray tube capable of rapidly switching between low and high tube potentials or two distinct X-ray tubes, each operating at different, fixed tube potentials. This capability of variable energy levels enhances the scanner's ability to produce more detailed images and improves the differentiation of various tissues and contrasts within the body.

2.2.8.2 Detector-Based Scanners

In contrast to source-based scanners, detector-based scanners rely on advanced detector technology that can resolve and distinguish between high-energy and low-energy X-ray photons. The detectors are designed to categorize incoming photons based on their energy levels, thus allowing for an enhanced interpretation of the imaged structures. This separation of energy levels is crucial for identifying various materials within the body, such as distinguishing between different types of calcifications in tissues or evaluating the composition of tumors.

Together, these two types of scanners represent the forefront of spectral CT technology, providing clinicians with innovative tools to obtain superior diagnostic information, ultimately leading to improved patient outcomes.

2.2.9 Dual-Source Imaging

Dual-source computed tomography (DSCT) represents a significant advancement in imaging technology, specifically in the field of cardiac diagnostics. A DSCT scanner is equipped with two separate X-ray tubes and two complementary detector systems, which are strategically arranged on a rotating gantry. These components are positioned with a 90degree angular offset from each other, allowing for enhanced imaging capabilities.

In DSCT systems, one of the X-ray tubes operates at a low energy setting (70 kV) while the other functions at a higher energy level (120 kV). This dual-energy approach not only improves image quality but also enhances the ability to differentiate between various tissue types, making it particularly useful in the evaluation of complex cardiac structures.

The primary advantage of DSCT is its superior temporal resolution, a crucial factor for effective cardiac imaging. This technology enables the acquisition of images with a temporal detail equal to just a quarter of the gantry's rotation time, which is approximately 83 milliseconds. This capability is maintained regardless of the patient's heart rate, providing consistent clarity and detail during imaging procedures. The scanner operates at a rotational rate of 0.33 seconds within a suitably centered scan field of view (SFOV), ensuring that images are captured swiftly and accurately, even during dynamic heart movements.

To optimize the utilization of the two X-ray tubes, DSCT can implement different acquisition techniques. For instance, the system can run both acquisition systems concurrently, allowing for extended scan lengths which is particularly beneficial for larger

patients or when conducting comprehensive examinations. These simultaneous operations can be carried out using either a sequential acquisition method or the standard helical method, as noted in the studies conducted by (Flohr et al., 2006, Flohr et al., 2008). This versatility in scanning techniques further enhances the efficiency and effectiveness of DSCT in clinical practice.

2.2.10 One-Source Scanning with Ultrafast Switching

The second type of spectral computed tomography (CT) employs a single X-ray tube that utilizes rapid kilovolt (kV) switching during a complete rotation of the gantry. During this process, the X-ray tube alternates between low and high tube potentials at a rapid pace. As a result, for each full rotation of the gantry, two comprehensive sets of projection data are acquired—one set at low kVp and the other at high kVp.

After obtaining these projections, advanced calibration and correction procedures are applied to convert the acquired data into the density of the materials represented by a chosen pair of base materials. These projections effectively indicate the mass of each material required to achieve the desired level of attenuation at the respective high and low kV settings.

To create a homogeneous energy projection, the process employs a weighted summation of the materials' densities, using their corresponding mass attenuation coefficients with a specific energy level acting as the weighting factor. This allows for a nuanced analysis of the materials' properties within the scanned volume.

Following this, a series of monochromatic images can be constructed, reflecting varying energy levels and density maps that correspond to the two basis materials. These images provide enhanced insights into the composition and distribution of materials within the scanned object, leading to improved diagnostic capabilities in medical imaging and material analysis (Li et al., 2011, Zhang et al., 2011).

2.2.11 Single Source & No Fast Potential Switches

One strategic approach to dual-energy imaging utilizing a single-source computed tomography (CT) scanner involves alternating the tube potential between gantry rotations in either an axial or helical (spiral) acquisition mode, rather than making adjustments within each gantry rotation. This method of acquisition, while functional, is generally considered to be less efficient compared to the rapid kV-switching technique.

This is particularly evident in applications focused on cardiac and abdominal imaging, where dynamic physiological processes such as respiratory patterns and the rhythmic beating of the heart could introduce significant variability between the two distinct energy projection sets generated over the two complete gantry rotations. Such inconsistencies can potentially compromise the reliability and accuracy of the imaging results (Chaytor et al., 2016, So and Nicolaou, 2021).

2.2.12 Split-Filter with One-Source Scan

Recently, several vendors have unveiled a groundbreaking imaging technique that enhances the capabilities of single-source X-ray scanners by employing a split filter positioned in front of the X-ray tube. This innovative method is designed to facilitate the generation of dual-energy projections, which is typically achieved through the use of dualsource systems.

The core concept behind this technique involves the use of a split filter that effectively separates the polychromatic spectrum emitted by the X-ray beam. The filter is constructed by stacking two distinct materials—gold and tin—side by side in a longitudinal arrangement. Each material has its unique attenuation properties, allowing the split filter to selectively absorb different energies of the X-ray spectrum.

By aligning this split filter correctly, the apparatus can extract valuable information from the dual-energy projections that are obtained from the single-source scanner. This advancement not only improves the quality of the imaging data but also offers potential benefits for a variety of applications in medical diagnostics, materials analysis, and other fields where precise imaging is essential (Euler et al., 2016).

2.2.13 Spectral Detector Computed Tomography (SDCT)

Spectral Detector Computed Tomography (SDCT) represents a cutting-edge advancement in imaging technology that combines the simultaneous collection of data at both low and high photon energy levels. This is achieved through the utilization of a duallayer detector system. The upper layer of detectors is designed specifically to capture lowenergy photons, while the lower layer is optimized for detecting high-energy photons. This innovative configuration allows for the effective segregation of low- and high-energy data, all of which is processed from a single X-ray tube operating under a unified potential.

One of the most significant advantages of SDCT is its rapid imaging capability, which contributes to a reduction in both the examination time and the overall radiation dose received by patients. Additionally, the use of SDCT minimizes the amount of contrast media required, enhancing patient safety and comfort during imaging procedures.

In terms of functionality, SDCT offers a range of capabilities that include the generation of mono-energetic Hounsfield unit (HU) spectral results, non-HU-based outcomes, modified HU spectral results, and uric acid removal (HU). The technique also facilitates virtual mono-energetic or monochromatic imaging (referred to as MonoE), which is derived from spectral computed tomography data. This approach significantly enhances soft tissue contrast, providing clearer images for diagnostic purposes, while also reducing common artifacts caused by beam hardening and scattering (Rassouli et al., 2017).

Furthermore, SDCT is designed to deliver comprehensive temporal and spatial resolution, ensuring that the captured images are not only detailed but also precise. This high level of resolution is crucial for accurately diagnosing various medical conditions and guiding effective treatment decisions.

Overall, Spectral Detector Computed Tomography stands at the forefront of imaging technology, offering clinicians powerful tools for improved diagnosis and patient management.

2.2.14 Clinical applications of spectral CT

Spectral-Detector Computed Tomography (SDCT) offers a diverse array of potential applications, particularly in the assessment of abdominal organs. It plays a vital role in the examination of the liver, adrenal glands, and kidneys by providing detailed imaging that aids in diagnosing various conditions affecting these organs.

One of the key advantages of SDCT lies in its sensitivity to detecting inflammatory conditions and ischemic bowel diseases. The technique is particularly beneficial for identifying subtle changes associated with weakly vascularized malignancies, such as pancreatic cancer. The variations in attenuation levels captured at different kilovolt peak (kVp) settings, specifically 80 kVp and 140 kVp, enhance the ability to differentiate various tissue types and pathological changes.

When imaging at 80 kVp as opposed to 140 kVp, the attenuation of vascular structures is consistently more pronounced. This increased contrast can significantly improve the detection and assessment of blood vessels during CT angiographic procedures. Furthermore, using a lower kVp has the added benefit of requiring less iodinated contrast material, which can reduce potential risks associated with contrast agent exposure while still providing highquality imaging.

Tissue characterization can be enhanced by spectral CT without requiring large amounts of contrast agents. By minimizing their use, patients can be exposed to less radiation and contrast because these agents frequently call for larger dosages or more frequent injections.

In summary, SDCT stands out as a crucial tool in abdominal imaging, facilitating detailed evaluations of key organs and enhancing the diagnosis of specific diseases through its ability to optimize contrast and attenuation (Adam et al., 2021).

2.2.15 Types of Images Generated from SDCT

2.2.15.1 Conventional Images

Conventional images, often referred to as routine diagnostic or polyenergetic images, play a crucial role in standard diagnostic procedures. These images are comparable in quality to those produced by single-energy scanning systems. The process involves utilizing two detectors to capture data at different energy levels—specifically high-energy and low-energy data.

In generating conventional images, the data from these two detectors is merged, allowing the layers to be visualized as if they were captured by a single detector. The raw data that results from this merging process undergoes complex reconstruction techniques. Two primary methods are employed for this purpose: iterative reconstruction methods and filtered back projection. These advanced approaches enable the creation of high-quality conventional images, which have been demonstrated to meet the diagnostic standards typically associated with single-energy scanners.

The resulting conventional images provide clinicians with valuable insights, maintaining a level of detail and clarity essential for accurate diagnoses. This advancement in imaging technology not only enhances the ability to detect various medical conditions

but also improves the overall efficacy of routine diagnostic procedures (Rassouli et al., 2017).

2.2.15.2 Spectral images

Are generated through the reconstruction of raw data derived from photoelectric and Compton scatter interactions. This process involves creating basis pair images that capture the different scattering events and their contributions to the overall spectral response. Additionally, these reconstructed images facilitate the generation of material composition images, which provide insights into the materials present in the scanned object.

To enhance the quality of the images produced, a beam-hardening correction is applied. This correction accounts for the variations in X-ray intensity as they pass through different materials, which can lead to artifacts in the images. Furthermore, the reconstruction chain incorporates advanced noise reduction techniques. These techniques are crucial for minimizing image noise, thereby improving the clarity and accuracy of the final spectral images. Overall, this comprehensive approach ensures that the resulting images are both reliable and informative for further analysis.

2.2.15.3 Images of Iodine Intensity

Images that depict iodine intensity display a detailed representation of iodine distribution within the scanned area. Each pixel in these images is assigned a value that reflects the concentration of iodine present, measured in milligrams per milliliter (mg/ml). Areas within the image that lack iodine appear dark, indicating no iodine presence. This technique is particularly useful for quantifying the distribution of iodine within various organs and arteries, allowing for a more accurate assessment of iodine uptake and localization. By utilizing iodine-only imaging, medical professionals can effectively analyze and interpret the iodine dynamics within the body, aiding in diagnostic and treatment planning processes.

2.2.15.4 Virtually Non-contrast Images

Virtually non-contrast images are specialized imaging outputs in which the contributions of iodine-based contrast agents have been effectively eliminated. As a result, the Hounsfield unit (HU) values assigned to the tissues within the pixels reflect the intrinsic density of those tissues without the influence of any contrast enhancement. This process results in images that closely mimic those obtained during standard non-contrast or precontrast scans, allowing for a clearer assessment of the underlying anatomy.

These images are particularly useful for evaluating conditions where the presence of a contrast agent may obscure critical details. Moreover, in cases like assessing uric acid deposits, which can be represented as distinct densities within the image, having a virtually non-contrast image can enhance diagnostic accuracy by providing a true representation of the tissue without the artifacts introduced by contrast agents (Rassouli et al., 2017).

2.2.15.5 Images of Uric Acid Pairs

Images of uric acid can provide valuable insights into the composition of urinary calculi and the diagnosis of gout. In a typical imaging result, the uric acid appears prominently, as the image displays only the pixels that correspond to the original Hounsfield Unit (HU) values specific to uric acid. The remaining pixels, which do not represent uric acid, appear black, creating a stark contrast that helps in visual identification.

Additionally, an accompanying image that highlights uric acid eliminated further enhances analysis by showcasing the regions where uric acid is absent. This complementary imaging technique allows for a clearer assessment of the uric acid's presence and helps differentiate it from other materials. Together, these images serve as essential tools for professionals in determining the specific composition of urinary stones and managing conditions such as gout, aiding in effective treatment planning and patient care.

2.2.15.6 Z effective images

Z-effective images are designed to visually represent the effective atomic number of various tissues within a given area. Each tissue is color-coded to provide a clear and immediate understanding of its unique composition. The coefficients associated with the photoelectric effect and Compton scattering are calculated meticulously as part of the spectrum decomposition process. These coefficients are influenced by the spatial distribution of the tissues, indicating how their arrangement impacts the interaction of x-rays or gamma rays. This detailed analysis allows for a better understanding of the underlying tissue characteristics and their response to radiation, enhancing diagnostic imaging techniques.

2.2.15.7 Virtual Monoenergetic Images (VMI)

The images were generated by utilizing a monoenergetic beam set at a specific energy level of one kiloelectron volt (keV). The resulting Velocity Map Imaging (VMI) was achieved through a linear combination of various basis pair images that were obtained within an energy range of 40 to 200 keV. This technique allows for a more comprehensive analysis of the interactions taking place at different energy levels, facilitating a clearer understanding of the underlying physical processes (Rassouli et al., 2017).

2.2.15.8 Virtual monoenergetic images with an equivalent

Virtual monoenergetic images (VMIs) can be generated to closely mimic the characteristics of images produced by a monoenergetic laser operating at a specific energy level, typically measured in kiloelectron volts (keV). These VMIs offer several advantages, including a significant reduction in noise and artifacts present in standard imaging techniques. Additionally, they achieve attenuation levels that are comparable to those found in conventional imaging methods, ensuring that the diagnostic quality remains high.

In terms of specific VMI values obtained from spectral detector computed tomography (SDCT), distinct energy levels are utilized for different regions of the body. For instance, a VMI value of 70 keV is applied for imaging the body's larger structures, while a slightly lower value of 66 keV is designated for the head to enhance detail in cranial imaging. Furthermore, for the extremities, an even lower VMI value of 64 keV is employed, optimizing the clarity and diagnostic information for these smaller limbs. These tailored energy levels help improve the overall accuracy and effectiveness of imaging across various anatomical regions.

2.2.16 Post-processing

The unique kVp switching technology is the only method that allows for the postprocessing of raw data in the projection domain to generate Mono-Energy (MonoE) datasets. This process, however, necessitates both angular and temporal interpolation to ensure accuracy in the reconstructed images. In contrast, other dual-energy computed tomography (DECT) systems available on the market operate based on different principles, primarily employing techniques such as beam hardening or modulation of the x-ray tube voltage.

When operating at low energy reconstruction levels, these alternative DECT systems typically produce MonoE reconstructions in the image domain rather than in the projection domain. This approach has a significant drawback: it results in markedly increased image noise, which can affect diagnostic quality. Consequently, the choice of technology in DECT systems is crucial, as it impacts the clarity and reliability of the resultant images, particularly when fine detail is critical in patient assessments (Doerner et al., 2017a).

2.2.17 Image Reconstruction Algorithms

The advancement of image reconstruction techniques in the field of CT has become increasingly important due to the need for high accuracy and efficiency, all while minimizing radiation exposure to patients. Over the past decade, rapid progress has been made in the development of mathematical algorithms specifically designed for CT imaging. This growth is indicative of the medical community's commitment to enhancing diagnostic imaging while prioritizing patient safety.

At the heart of CT image reconstruction lies the challenge of determining the attenuation coefficients associated with different X-ray absorption pathways. These coefficients are derived from a collection of data known as projections, which represent the X-ray intensity measurements obtained from various angles around the object being scanned.
The reconstruction process aims to convert these projections back into a visual representation of the internal structures of the object, typically a human body (Seeram, 2015).

Numerous algorithms have been developed and implemented for the reconstruction of CT scans. Among these, three of the most widely recognized and commercially available algorithms include: Filtered Back Projection (FBP), Iterative Reconstruction (IR), and Model-Based Iterative Reconstruction (MBIR).

2.2.18 Filtered Back Projection

This is one of the oldest and most commonly used methods for CT image reconstruction. The FBP technique involves applying a mathematical filter to the raw data collected from the projections before back-projecting them onto a grid to form the image. While it is efficient and fast for generating images, FBP may struggle with noise and artifacts, particularly in low-dose scans.

Filtered Back Projection (FBP) is a well-established image reconstruction method predominantly used in CT imaging. This technique employs a filtering process known as convolution, which is specifically designed to eliminate blurriness inherent in traditional back-projection methods. As a result, FBP has become the primary approach for reconstructing cross-sectional images in CT scans (Seeram, 2015).

One of the notable advantages of using FBP is its ability to facilitate focused and precise image reconstruction. The algorithm applies smooth weighting functions that are particularly beneficial when the object being scanned exhibits movement during the imaging process. FBP operates under certain assumptions, including the use of a point detector and pencil x-ray beam geometry, which allow for rapid reconstruction of images. This efficiency makes FBP suitable for a wide range of clinical situations, contributing to its popularity in medical imaging.

However, despite its effectiveness and user-friendliness, the limitations of FBP become increasingly apparent, especially in specific contexts. When the radiation dose is reduced—often due to the need for minimizing patient exposure or in the case of larger patients—FBP tends to produce images that exhibit increased noise and artifacts. This phenomenon occurs because FBP relies on simplified approximations of the CT raw data, also referred to as a sinogram. A sinogram is essentially a comprehensive collection of various projections acquired from different angles for each imaging sector (Nuyts et al., 2013).

The shortcomings of FBP can be attributed to its inability to incorporate measurement errors that stem from the nonideal characteristics of the CT system, such as detector crosstalk and beam hardening. These factors can lead to inaccuracies in the reconstructed images. In contrast, iterative reconstruction (IR) techniques offer a solution by effectively reducing image noise and enabling CT protocols to be performed at lower radiation doses compared to those using filtered back projection. IR approaches involve multiple iterations of image estimation and refinement, improving both image quality and diagnostic utility.

Overall, while FBP remains a foundational technique in CT imaging, the evolution towards more advanced methods like iterative reconstruction signifies a crucial step in enhancing image quality and patient safety in diagnostic radiology.

2.2.19 Iterative Reconstruction (iDose4)

Unlike FBP, iterative reconstruction techniques take a more sophisticated approach by repeatedly refining an initial estimate of the image. This method incorporates statistical models and prior knowledge of the object being scanned, allowing for improved image quality and reduction of noise. IR has become increasingly popular due to its ability to enhance image clarity even at lower radiation doses.

The first iterative reconstruction tool made available commercially by Philips Healthcare, iDose4, is a hybrid iterative reconstruction algorithm that combines two denoising components: a local structure model fitting on image data that iteratively reduces noise, and an iterative maximum likelihood-type sinogram restoration based on Poisson noise distribution. The degree of noise reduction is determined by the iDose levels (1–7), whereby raising the level corresponds to a higher percentage of noise reduction (Khawaja et al., 2014, Yuki et al., 2016).

The features of iDose reconstructions above FBP showed no streak artifacts, proving that noise in the projection domain can be properly treated to avoid any streak artifacts in the image reconstructions. Also, when an artifact is corrected, there is no loss of resolution. An additional advantage of hybrid iterative techniques is the prevention of bias as opposed to the previous reconstruction.

Fourth-generation methods iDose4 maintain the image's texture and "natural look" by improving the efficiency of noise reduction over the whole noise spectrum. iDose4 offers a novel approach that carries out iterative processing in the projection and image domains.

The reconstruction technique finds and corrects those noisiest CT findings using projection data as an initial basis. Edges are conserved and noisy data are penalized by an iterative diffusion process.

The iDose4 algorithm's next significant part works with eliminating image noise while keeping the underlying edges connected to actual anatomy or pathology. After that, a selection selects noiseless structural models, and the model that most closely matches the image volume's local geometry is selected. After selecting the optimal model, the noise in the image volume is reduced. The noise in the image volume is decreased after the optimal model has been selected. It can choose from seven different levels to change the noise reduction strength. Level 1 should theoretically reduce noise by 11%, while level 7 translates to a 55% reduction in noise.

According to the vendor, iDose4 The fourth stage can get dosage decreases of up to 80% (Osorioa and Namíasb). Finally, iDose4 allows for a considerably reduced radiation dose without impacting the quality of the diagnostic image (Healthcare, 2011). The limitation of this reconstruction is that may change noise texture. Also, iDose4 configurations require additional modification. A deeper comprehension of the usage of iterative algorithms in clinical practice may be possible with the help of published information.

2.2.20 Iterative Model Reconstruction (IMR)

The second-generation iterative reconstruction (IR) technique known as Iterative Model Reconstruction (IMR) has been developed by Philips Healthcare, building upon the previous hybrid IR method, iDose4. IMR represents a significant advancement in imaging technology, as it operates through a sophisticated iterative cycle that intricately considers various factors including image noise patterns, data statistics, image statistics, and advanced system models.

IMR is categorized into three distinct levels of noise reduction. As one progresses to higher levels, the extent of noise reduction increases, allowing for tailored image quality based on clinical requirements. The process formulates image reconstruction as an optimization problem, where the goal is to minimize a cost function. This cost function incorporates several critical elements: the geometry of the imaging system, a noise model that reflects true photon detection statistics, and a regularization term that serves to penalize noisy solutions produced during the iterative process.

In practical terms, an iterative procedure is employed to identify the image that minimizes this cost function, which is integral to achieving enhanced image quality. According to claims by the manufacturer, the IMR technique can yield remarkable results, including noise reduction between 70% and 83%, improvement in low-contrast detectability ranging from 40% to 80%, and significant dose reductions of 60% to 80%, depending on various factors such as the clinical task, patient size, anatomical location, and specific clinical practices (Osorioa and Namíasb et al., 2019).

The IMR process effectively integrates multiple domains: optics—encompassing the x-ray source, image voxels, and detector; noise characterized by photon statistics; the physics underlying data acquisition; and the anatomical considerations of radiation attenuation. This holistic approach not only aids in the formation of highly detailed illustrations of the scanned object but also enhances the utility of photon information and CT system models simultaneously.

Importantly, IMR shows exceptional capabilities in improving tumor conspicuity and overall image quality, especially when imaging patients at reduced radiation doses. Research findings reveal that IMR significantly boosts tumor conspicuity and increases the contrastto-noise ratio (CNR), outperforming both Filtered Back Projection (FBP) and iDose4 techniques in the visualization of low-contrast focal lesions. Furthermore, IMR substantially decreases image noise, achieving reductions ranging from 59.5% to 79.6% compared to iDose4 (Kulkarni et al., 2021a).

To achieve its advanced imaging outcomes, IMR utilizes a global statistical and system model-based approach that uniquely tailors to the specific CT scanner in use. This system takes into account crucial parameters such as focal spot size, beam width, voxel size, detector pixel size, and the interactions between the beam and detector.

The iterative minimization of a cost function, which includes a pre-regularization fee, is a fundamental aspect of the IMR technique. Long-term studies demonstrate that IMR effectively enhances the visibility of thoracic structures by eliminating imagined noise and artifacts, thereby facilitating improved diagnostic assessments. Consequently, low-dose CT scans utilizing the IMR technique can be particularly beneficial for accurately identifying lung lesions (Yuki et al., 2016).

Despite its advantages, IMR is not without limitations. Radiologists may perceive IMR images differently than those produced by FBP or iDose methodologies. However, with familiarity, radiologists might leverage the lower noise levels of IMR images to further reduce radiation dosage while maintaining diagnostic efficacy. Additionally, a notable challenge associated with hybrid iterative reconstruction (HIR) methods is their often slow reconstruction speeds, which can impact clinical workflow and efficiency (Mehta et al., 2013).

2.2.21 Factors Affecting Image Quality in CT

2.2.21.1 CT Imaging Parameters

The quality of images produced by CT systems is influenced by a range of technical parameters that directly impact their performance in terms of detectability and diagnostic effectiveness. Key factors include the specifications of the CT system, the milliamperesecond (mAs), peak kilovoltage (kV), slice thickness, pitch, beam collimation, alongside various image processing techniques and visualization methods. Each of these

variables plays a critical role in optimizing image quality while simultaneously striving to minimize the radiation dose administered to the patient.

2.2.21.2 Signal-to-Noise Ratio (SNR)

Is a crucial metric that directly correlates with image quality. To enhance image quality, it is often necessary to increase the SNR; however, this generally entails raising the radiation exposure to the patient. Research indicates that to improve the SNR by a factor of 1.4, it may require the radiation dose to be doubled, which poses significant concerns regarding patient safety (Falck et al., 2010). Therefore, the determination of allowable radiation doses is contingent upon the specific clinical context and the anticipated benefits of the high-dose procedure, which is typically discouraged.

As mAs are reduced, there is a concomitant increase in image noise, which compromises the clarity of the images and decreases the contrast-to-noise ratio (CNR). Lowering the mAs inevitably decreases the number of X-ray quanta reaching the detector, which adversely affects the visualization of anatomical structures, leading to potential diagnostic difficulties (Toth, 2012). Additionally, there is a fundamental trade-off between radiation dosage and spatial resolution. Higher spatial resolution often necessitates an increase in radiation exposure (Özgün et al., 2005). Therefore, it is essential to consider the specific diagnostic objectives and clinical tasks at hand when evaluating the acceptable tradeoffs between image quality and radiation dose (Seibert, 2004).

To enhance image quality while managing radiation exposure, increasing the milliampere-second (mAs) settings is one strategy to lower noise levels. However, to maintain optimal image quality, careful adjustments to mAs must be made to keep radiation doses as low as reasonably achievable (Alsleem and Davidson, 2013). Furthermore, employing lower kilovoltage values can lead to improved photoelectric interactions, which increases attenuation levels within the tissue being imaged. This, in turn, enhances both

image contrast and detail sensitivity, contributing to better diagnostic outcomes (Båth, 2010).

In conclusion, effectively balancing these various parameters is crucial for achieving high-quality CT images while ensuring patient safety through minimized radiation exposure.

2.2.22 Radiation Risk

The biological effects of ionizing radiation are classified into two main categories: deterministic and stochastic effects. Deterministic effects occur when the radiation dose exceeds a specific threshold, leading to measurable harms that escalate in severity with increasing doses. Common examples of deterministic effects include skin damage, such as erythema and desquamation, as well as cataract formation in the lens of the eye. In contrast, stochastic effects are characterized by their probabilistic nature; these effects, such as the development of cancer or germ cell mutations, arise randomly and become more likely as the dose of radiation increases, without a defined threshold.

It is widely recognized that enhancing image quality in computed tomography (CT) imaging can be achieved by increasing radiation exposure, as this typically leads to a reduction in noise levels within the images produced (Marin et al., 2009). However, this approach raises significant concerns given the potential risk of radiation-induced cancer related to CT scans. Despite the critical role that CT imaging plays in providing essential diagnostic information and improving healthcare outcomes, the associated risks cannot be overlooked (Phase, 2006).

Consequently, a core focus of ongoing research and clinical practice is the optimization of radiation doses during CT examinations. The objective remains to reduce the amount of radiation exposure while maintaining or even enhancing the overall image quality. Innovations in CT scanners—such as advanced algorithms and refined imaging

techniques— are instrumental in achieving these goals. Most notably, a more measured approach to radiation dose reduction is often adopted in specific scenarios like oncologic imaging, where the priority might shift to enhancing image quality while utilizing standard radiation doses (Wichmann et al., 2017, Larbi et al., 2018).

Radiation doses received by patients during CT scans can be quantified using several metrics, including the Computed Tomography Dose Index (CTDI), the weighted CTDI (CTDIw), the volume CTDI (CTDIvol), the multiple scan average dose (MSAD), and the dose-length product (DLP). Among these, CTDI and DLP are the most recommended for representing CT dose and informing best practices.

CTDI serves as a critical physical measurement that quantifies the radiation output per slice from CT scanners. It incorporates factors such as the geometric configuration of the Xray beam, including the focal spot size and collimation, as well as the type of filtering applied during the scan (Shope et al., 1981). As technology has advanced, the volume CTDI (CTDIvol) has become increasingly available, offering real-time feedback on the radiation dose delivered based on the selected scan parameters. This immediate data is vital for radiologists, enabling them to assess and adjust the dosing as needed to ensure patient safety while still achieving diagnostic objectives (Imhof et al., 2003).

2.2.23 Radiation Risk CT Spectral Detector

Many variables, such as the particular scan protocol, the technology employed, the patient's size, and the clinical indication, affect the radiation risk of spectral detector CT. Nevertheless, in order to better appreciate the relative danger, it is important to compare the radiation dose of spectral CT with standard CT.

2.2.26.1 Dose of Radiation Concerning Traditional CT

Compared to standard CT, spectral CT usually utilizes less radiation. This is due to spectral CT technology's ability to make use of dual-energy imaging, which can assist decrease the need for several scans and increase the precision of diagnosis. When compared to traditional CT, spectral CT can sometimes provide the same or even better diagnostic results while lowering radiation exposure. As an illustration, photon-counting detectors enable better image quality at lower radiation dosages (Greffier et al., 2023).

To further minimize needless radiation exposure, modern spectral CT systems can more accurately modify the radiation dose depending on the size of the patient and the area being scanned (Brady et al., 2021).

With the utilization of a wider energy spectrum, spectral CT can optimize imaging energy and enhance signal-to-noise ratios, potentially enabling lower dosage scans without sacrificing image quality.

2.2.24 Comparison with Traditional CT

The radiation dose in a traditional CT scan might vary significantly based on the patient's size and the scan region (head, chest, or abdomen). Effective dose (measured in millisieverts, mSv), which ranges from 1 mSv for a head CT scan to 10 mSv for an abdominal CT scan, is frequently used to quantify the risk of radiation-induced cancer.

Spectral CT seeks to decrease this dosage by increasing the effectiveness of imaging. According to recent research, dual-energy and spectral CT can provide comparable or better diagnostic outcomes with up to 40–60% less radiation than single-energy CT (Sauter et al., 2020).

2.2.25 Similar Studies

In a study conducted by Funama et al. (2014), the researchers aimed to compare the levels of noise and accuracy in liver images obtained through two different reconstruction

methods: iterative model reconstruction (IMR) and filtered back projection (FBP). This investigation involved acquiring 100 liver CT images, where in the standard deviation (SD) and mean of the noise levels were meticulously measured. The results indicated that the SD for the FBP technique was notably higher, suggesting that it produced noisier images. In contrast, images reconstructed using IMR at level 3 exhibited the lowest SD, implying that the accuracy of the imaging increased with IMR3, resulting in clearer and more reliable liver scans (Funama et al., 2014).

Similarly, Kayal et al. (2019) focused on evaluating the effectiveness of a novel spectral detector-based computed tomography (SDCT) scanner in assessing various types of pancreatic lesions. The study included 61 patients diagnosed with pancreatic lesions from different anatomical locations and involved imaging these lesions using abdominal SDCT with the administration of contrast media.

Two experienced radiologists analyzed the resultant images, using a 5-point Likert scale to evaluate the quality and accuracy of diagnoses for several reconstruction techniques, including conventional polyenergetic reconstructions (polyE), virtual (monoE), virtual noncontrast images, iodine density images, iodine overlay images, and Z-effective (Zeff) maps. The analysis revealed that images reconstructed with low kiloelectron volt (keV) monoE produced the highest Likert ratings in terms of reader confidence and the conspicuity of tumors. The findings concluded that spectral detector CT significantly enhances the visibility of pancreatic tumors, although the authors noted a need for further research to determine its clinical implications in larger populations (El Kayal et al., 2019).

Li et al. (2021) sought to investigate the utility of SDCT in differentiating between focal nodular hyperplasia (FNH), hepatic hemangioma (HH), and hepatocellular carcinoma (HCC). This retrospective study included 51 patients who underwent multiphase spectral CT scans within a keV range of 40 to 140. The research involved extracting quantitative

data, including normalized iodine concentration, iodine uptake ratio (IUR), iodine density, and water density, through iodine-based and water-based material breakdown images. The study concluded that CT measurements could considerably aid in distinguishing between HCC, HH, and FNH at lower energy levels (40–90 keV), highlighting the potential of SDCT in enhancing diagnostic accuracy for liver lesions (Li et al., 2021).

Shapira et al. (2020) investigated the incremental value of spectral CT data over conventional CT for fully automated liver lesion localization and diagnosis. Utilizing a spectral dual-layer CT scanner, both conventional and spectral CT images, including virtual monochromatic images (VMI), were generated.

The analysis of clinical reports provided insights into the patient's diagnosis, categorizing lesions as hypodense metastases, cysts, or healthy tissue. Measurements indicated that the distances for localization using iodine maps, 40 keV VMIs, and 70 keV VMIs were 8.22 ± 10.72 mm, 8.78 ± 15.21 mm, and 8.29 ± 12.97 mm, respectively. The study found that the 40 keV VMIs yielded the highest accuracy at 0.899, compared to 0.854 for traditional data. The findings suggest that spectral CT data could significantly improve both diagnostic accuracy and clinical workflow in liver imaging (Shapira et al., 2020).

Kulkarni et al. (2021) compared the effectiveness of iterative model reconstruction (IMR) with low-dose and hybrid iterative image reconstruction techniques in CT scans aimed at evaluating tumor visibility and image quality in patients with liver diseases, such as cirrhosis and hepatocellular carcinoma. By measuring signal-to-noise ratio (SNR) and contrast-to-noise ratio (CNR), their results demonstrated that IMR provided superior image quality compared to Idose4 in all liver disease cases examined. Furthermore, the low-dose IMR technique resulted in a remarkable 36% reduction in image noise compared to Idose4,

supporting the conclusion that the IMR algorithm offers significantly enhanced imaging capabilities even when employing low-dose protocols (Kulkarni et al., 2021a).

Laqmani et al. (2016) conducted a study utilizing two distinct iterative reconstruction (IR) algorithms—iDose4 and IMR—to assess image quality in CT pulmonary angiography (CTPA) executed with reduced radiation exposure (RD-CTPA) and minimized contrast medium volume, comparing their outcomes to those obtained from traditional filtered back projection (FBP). Quantitative analysis revealed that IMR significantly outperformed the iDose4 algorithm in terms of noise reduction, achieving noise reductions of up to 85% compared to FBP, and 66% when compared to iDose4. Additionally, IMR produced the highest CNR estimates, further solidifying its efficacy in providing clearer images than both FBP and iDose4 (Laqmani et al., 2016b).

Medina et al. (2019) presented findings from the acceptance tests of a Philips iCT Elite scanner equipped with the iterative model-based IMR reconstruction algorithm. This study also examined the influence of various reconstruction techniques—including IMR, iDose4, and FBP on image quality at different radiation dose levels. Using a Catphan 500 phantom, the researchers measured CT numbers for multiple materials, yielding results that aligned closely with predicted values.

The study found that IMR reconstructions improved low-contrast detectability by 50% and reduced image noise by 75% when compared to both FBP and iDose4, without compromising high spatial contrast resolution (HSCR). These findings confirmed the effectiveness of IMR in enhancing overall system performance and image quality, serving as a benchmark for regular quality assurance practices within the imaging facility.

In a study conducted by Mu et al. (2022), the team addresses the challenges faced in using conventional CT to accurately determine the pathological grade of lung adenocarcinoma (LUAD). The primary objective of this research was to evaluate tumor differentiation by utilizing a combination of morphological factors and advanced imaging techniques with a dual-layer spectral detector CT. The study involved a prospective analysis of 67 patients who had been pathologically diagnosed with LUAD. Among these patients, 28 were categorized into the poorly differentiated group, while the remaining 39 were classified as belonging to the well-differentiated and moderately differentiated groups, comprising 14 and 25 patients, respectively.

The researchers meticulously measured various tumor morphological features, which included analyzing the monoenergetic CT images at energy levels of 40 and 70 keV, assessing iodine density within the tumors and the thoracic aorta, as well as examining the non-enhanced and double-enhanced CT numbers. Additionally, they evaluated the effective atomic number of the tumors. The conclusion drawn from this study indicates that the pathological grade of LUAD can be effectively distinguished by leveraging the unique characteristics captured by the dual-layer spectral detector CT.

Notably, they found that the normalized iodine density measured during the arterial phase emerged as the most diagnostically effective spectral metric. Furthermore, integrating spectral data with morphological characteristics significantly enhances the accuracy of pathological grading for LUAD (Mu et al., 2022).

Another relevant study by Yuan et al. delves into the determination of the optimal energy level for imaging pancreatic neuroendocrine neoplasms (pNENs) using dual-layer spectral detector computed tomography (DLCT). This retrospective analysis encompassed 134 patients with 136 distinct lesions, all of which had undergone contrast-enhanced DLCT

scanning and had their pNENs validated through histopathological assessment. The research involved a comprehensive evaluation of various imaging types, including conventional images, Z-effective atomic number maps (Zeff maps), iodine concentration maps (IC maps), and virtual monoenergetic images (VMI) within an energy range of 40 to 100 keV.

The researchers compared signal-to-noise ratios (SNR) and contrast-to-noise ratios (CNR) to identify the optimal energy level for imaging. They also analyzed lesion detection rates between DLCT and traditional imaging modalities. Two independent readers performed subjective assessments of the images using a 5-point rating scale to evaluate aspects such as overall image quality and lesion conspicuity. The findings from this study indicate that DLCT serves as a valuable tool for assessing pancreatic lesions, revealing that, within the range of virtual monoenergetic images, VMI images at 40 keV demonstrate the highest objective image quality.

Moreover, the spectral images obtained from DLCT showed a remarkable capability in detecting lesions: with a diagnostic accuracy of 100% for lesions larger than 15 mm and 90.5% for those smaller than 15 mm, surpassing traditional imaging techniques. In subjective evaluations, the performance of DLCT—specifically the VMI 40 keV, IC map, and Zeff map—was superior to that of conventional CT in terms of tumor conspicuity and the delineation of margins (Yuan et al., 2023).

The second approach was U-Net, which is based on convolutional neural networks. With hand segmentation serving as the reference standard, both approaches were contrasted with equivalent algorithms that employed traditional CT attenuation. agreement with the reference standard was evaluated. They found that applying the algorithms to SDCT data produced better segmentation results than applying the same algorithms to traditional CT data (Ng et al., 2020).

Chapter Three: Methodology

3.1 Patient selection

This retrospective study was conducted with selective patients, mainly from the patients' friend's society-Al-Rahma Hospital between July and September 2023. The patients included in this study had been previously imaged using Spectral CT 7500 from Philips company and they were reported by one of the following diseases in the liver region such as metastatic lesions, hemangiomas, and fatty liver. The distribution of the cases is shown in Table 3.1.

Table 3.1: The distribution of liver disease cases.

	Pathology	Gender	Age
Patient 1	Metastasis	Female	52y
Patient 2	Metastasis	Female	60y
Patient 3	Metastasis	Female	62y
Patient 4	Metastasis	male	71y
Patient 5	Metastasis	Female	47y
Patient 6	Hemangioma	male	67y
Patient 7	Hemangioma	Female	63y
Patient 8	Hemangioma	male	63y
Patient 9	Hemangioma	male	22y
Patient 10	Hemangioma	Female	48y
Patient 11	Fatty liver	Female	65y
Patient 12	Fatty liver	Female	38y
Patient 13	Fatty liver	male	10y
Patient 14	Fatty liver	male	54y
Patient 15	Fatty liver	Female	36y
Patient 16	Fatty liver	Female	49y

3.2 CT Imaging Protocol

The CT images available at the picture archiving and communication system (PACS) were retrieved for the 16 patients and were then reconstructed by two main reconstructions which are innovative dose reduction techniques (iDose) and Iterative Model Reconstruction (IMAR). Each image was reconstructed with two levels, level 2 and level 4 for iDose reconstruction and level 1 and level 3 for IMAR reconstruction. To test the effect of tube voltage in the assessment of different pathology, two tube voltages were used in the virtual CT system including low tube voltage and high tube voltage of 70 keV and 120 keV, respectively. Therefore, eight combinations were obtained as shown in Table 3.2. The reconstruction type and the value of keV were used in the study.

Table 3.2: The reconstruction type and the value of keV were used in the study

Reconstruction techniques	iDose2	iDose4	IMR1	IMR3
keV value	70 keV		70 keV	
	120 keV		120 keV	
Output of image reconstructed	iDose2 70keV		IMR1 70keV	
	iDose2 120keV		IMR1 120keV	
	iDose4 70keV		IMR3 70keV	
	iDose4 120keV		IMR3 120keV	

3.3 Radiologist Assessment

Three experienced radiologists, each with a minimum of 8 years of expertise, meticulously analyzed a total of eight combinations of CT images post-reconstruction. Each radiologist diligently scrutinized a substantial amount of 128 scans across 16 patients. Throughout this comprehensive evaluation process, high-quality, high-resolution monitors were utilized to ensure accurate assessments. The primary focus of their evaluation centered

around the axial reconstructed images within the clinical environment. Adhering to predefined guidelines, they meticulously concentrated their attention on the perceived sharpness, contrast, and characterization of lesions within the scans.

It's worth noting that radiologists employed a systematic approach, following established protocols to maintain consistency and precision in their evaluations. The specific emphasis on sharpness, contrast, and lesion characterization was crucial in facilitating accurate diagnoses of liver diseases. Furthermore, to standardize the evaluation process and ensure uniformity in scoring, a 5-point Likert scale was utilized to quantitatively assess the overall image quality in diagnosing various liver conditions.

This scoring system, as detailed in Table 3.3, provided a structured framework for radiologists to rate the images consistently and effectively based on their perceived quality and diagnostic value. Through this methodical and meticulous approach, the team of radiologists aimed to optimize the diagnostic accuracy and reliability of their assessments for the benefit of patient care and treatment outcomes.

Table 3.3: 5-point Likert scale to assess SDCT image quality

Rating	Description
Score 1	Insufficient image quality
Score 2	Poor image quality
Score 3	Moderate image quality
Score 4	Good image quality
Score 5	Excellent image quality

3.4 Image Quality Assessment

Signal-to-noise ratio (SNR) and contrast-to-noise ratio (CNR) were utilized as evaluation metrics to assess the quality of CT images based on eight different combinations

acquired during the study. To determine the Hounsfield Units (HU), circular regions of interest (ROIs) consisting of 20 pixels were meticulously drawn on three distinct normal locations within the liver CT images.

These same ROIs were then replicated in the center of the lesion to measure the HU value for each area, as depicted in both Figure 1 and Figure 2. Subsequently, the SNR was calculated through specific equations designed for this purpose, taking into account the variations in noise and signal strength in the images captured for analysis.

Normal SNR= average HU liver/SD liver...........(Yang et al., 2023)

Abnormal SNR=HU lesion/SD liver............(Yang et al., 2023)

Normal CNR= HU liver-HU muscle/SD muscle............(Yang et al., 2023)

Abnormal CNR= HU lesion-HU muscle/SD muscle............(Yang et al., 2023)

SNR and CNR were calculated for fatty liver diseases in the eight reconstructed CT images as shown in Figure 3.1 and calculated using the following equations:

Abnormal SNR= HU lesion/SD liver............(Yang et al., 2023)

Abnormal CNR= HU lesion-HU muscle/SD muscle.............(Yang et al., 2023)
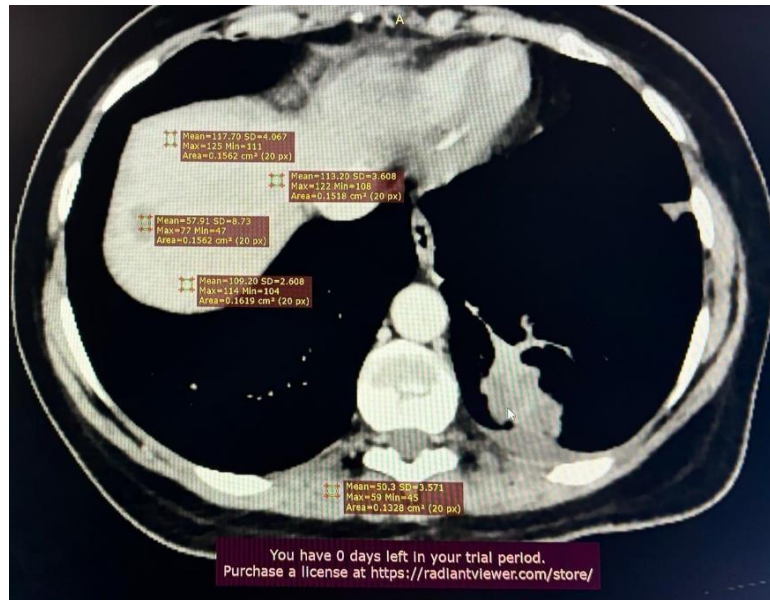
Figure 3.1: Axial view for liver CT scan for a patient with metastatic liver disease.
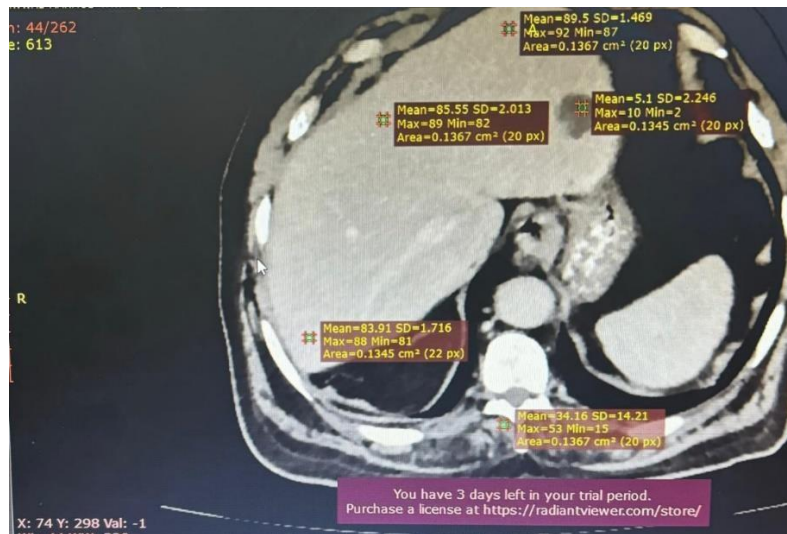
Figure 3.2: Axial view for liver CT scan for a patient with hemangiomas liver disease
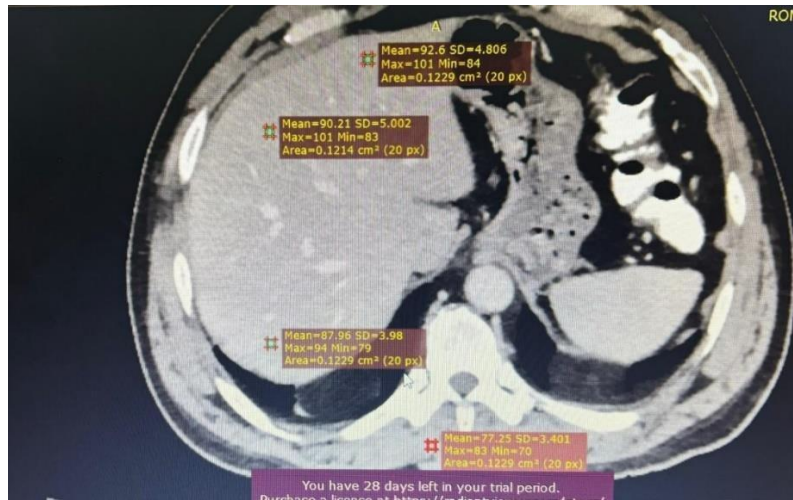
Figure 3.3: Axial view for liver CT scan for a patient with fatty liver disease.

3.5 Dose measurement

To thoroughly evaluate the radiation dose received from the abdomen and pelvis examination spectral CT scan, the team conducted a comprehensive analysis by measuring the CTDI value for the system. This value was then meticulously compared with the corresponding data available from MDCT scans using a 64-slice detector of the same brand. All these intricate measurements were carried out using a body CT phantom designed to mimic a realistic human body structure, specifically a PMMA cylinder with a diameter of 32 cm for body scans. The initial radiation dose measurement for the Philips MDCT 64-slice scanner was successfully procured and is accessible at Rafidia Governmental Hospital for reference.

Furthermore, the parameters and measurements that were utilized as the standard for the abdomen and pelvis CT examination are systematically detailed in Table 3.4. Table provide a comprehensive overview of the specific settings and values employed during the imaging process, ensuring consistency and accuracy in the examination procedures. By adhering to these standardized protocols and meticulously recording all relevant data, the team aims to enhance the reliability and precision of the radiation dose assessment for

abdominal and pelvic CT scans using spectral CT technology. This diligent approach not only ensures the validity of the findings but also facilitates comparative analyses with existing literature and clinical practices, thereby contributing to the broader advancements in diagnostic imaging techniques and radiation safety protocols.

Table 3.4: The parameters used based on a standard abdomen pelvis MDCT examination

Parameters	Value
Chamber normalization factor	1
kVp	120
Exposure time in (sec)	4.1
mAs	378
Pitch	0.75
Slice thickness	2 mm

The same procedures were done for a spectral CT scan (Philips scan 256-slice) available at Patients Friends Society-Al-Rahma Hospital while the parameters used for the system are shown in Table 3.5.

Table 3.5: The parameters used to measure radiation dose in SDCT

	Chamber normalization factor	1
	kVp	120
Parameters	Exposure time in (sec)	1
	mAs	157
	Pitch	1
	Slice thickness	2 mm

The CTDI 100, CTDIw, and CTDI vol were the standard values based on the following equations for comparison purposes.

CTDI w= 1/3(CTDI100) centers + 2/3 (CTDI100) peripheral. ....(McNitt-Gray, 2002)

CTDIv = CTDIw/pitch ....(McNitt-Gray, 2002)

3.6 Statistical Analysis

In the data analysis phase, the statistical software SPSS (version 26 for Windows, USA) played a central role by facilitating the computation of means and standard deviations (SD). These calculations served as crucial metrics in the evaluation of liver CT images to distinguish between normal and abnormal cases, particularly focusing on assessing the SNR and CNR related to metastasis lesions and hemangiomas. Additionally, the SNR and CNR for abnormal fatty liver were also examined. The descriptive statistics encompassed an extensive comparison of eight parameters derived from evaluations conducted by three different raters.

To explore the relationship between doses within the same reconstruction, Pearson correlation analysis was employed. Notably, the Pearson correlation coefficient (r) ranges provided a framework for interpreting the level of agreement, classifying values between 0.2 and 0.39 as weak, 0.4 to 0.59 as moderate, and 0.6 to 0.79 as strong.

Furthermore, the percentage difference for SNR data was meticulously computed to highlight variations, while statistical significance was determined using a significance level of 0.05 through the analysis of P-values. These methodical analyses and assessments were instrumental in gaining valuable insights into the imaging data, ultimately contributing to a comprehensive understanding of the study's outcomes.

Chapter Four: Results

4.1 Relation of Reconstruction Algorithm and Tube Voltage

The Pearson correlation and p-value for the same reconstruction techniques but different keV values as obvious in Table 4.1, there is a positive relationship when the tube voltage increases from 70 keV to 120 keV when compared between the reconstruction technique IMR3 with 120 keV and IMR3 with 70 keV, that looks to have the highest value because the Pearson correlation is 0.789 which means that there is a strong positive correlation and it is statistically significant the p-value is 0.000. The reconstruction technique IDOSE2 with 120 keV and IDOSE2 with 70 keV have the lowest value, the Pearson correlation was found to be 0.291 which means that there was a weak positive correlation with p-value 0.045.

Table 4.1: IMR and IDose Reconstructions techniques with its correlation with tube voltages.

Reconstruction techniques	Pearson Correlation	P Value
IMR1 120keV VS IMR1 70keV	0.462 (**)	0.001
IMR3 120keV VS IMR3 70keV	0.789 (**)	0.000
IDOSE2 120keV VS IDOSE2 70kev	0.291 (*)	0.045
IDOSE4 120keV VS IDOSE4 70keV	0.390 (**)	0.006

4.2 Imaging Assessment of Metastatic and Hemangioma Cases

Based on statistical analysis, it was found that the reconstruction technique IMR3 has the highest value among normal, abnormal SNR, and normal CNR as shown in Table 4.2. The mean and standard deviation for normal SNR of IMR3 combined with 70 keV and 120

keV were found to be 38.92 ± 14.04, and 46.4 ±19.05, respectively. While the lowest value for normal SNR was found using IDOSE2. For IDOSE 2 combined with 70 keV was found 7.56 ± 2.36, and 120 keV was found to be 7.42±2.87. The second parameter that has been calculated is abnormal SNR where the IMR 3 reconstruction combined with a low energy level was found 21.83±19.5 but with a high energy level was found 21.47±16.83. Also, the lowest value for abnormal SNR was in IDOSE2. The IDOSE 2 (70 keV) showed a value of 3.51±2.02 in contrast, IDOSE 2 (120 keV) 3.21±2.23. The IMR3 in normal CNR with 70keV was 13.63±11.39, but in 120keV was found 11.32±7.69. The lowest CNR value was found using IDOSE2. For the abnormal CNR, the IMR3-70 (2.11±7.86) was found higher compared to IMR1-70 (-0.47±6.15) while in comparison with 120 keV energy, the IMR1 showed a higher value (0.72±4.51) compared with IMR3 with same energy level (-0.23±7).

Table 4.2: Descriptive statistics for various tube voltage and image reconstruction for patients with metastatic and hemangioma

Parameters	70 keV protocol				120 keV protocol			
	IMR1	IMR3	IDOSE2	IDOSE4	IMR1	IMR3	IDOSE2	IDOSE4
Normal SNR	23.18±11.29	38.92±14.04	7.56±2.36	9.6±3.77	20.53±5.20	46.4±19.05	7.42±2.87	16.70±24.22
Abnormal SNR	9.93±5.45	21.83±19.5	3.51±2.02	4.36±2.61	8.87±5.64	21.47±16.83	3.21±2.23	4.07±2.72
Normal CNR	10.14±5.74	13.63±11.39	4.15±1.73	4.61±1.73	8.68±4.81	11.32±7.69	3.88±1.4	4.57±2.25
Abnormal CNR	-0.47±6.15	2.11±7.86	0.32±1.34	0.29±1.77	0.72±4.51	-0.23±7	-0.0±2.03	0.57±1.91

The percentage difference for normal and abnormal SNR for IMR1, IMR3, IDOSE2, and IDOSE4 is shown in Table 4.3. In normal SNR, IDOSE4 showed the highest percentage difference (53.99%), while IDOSE2 was the lowest (1.87%). In abnormal SNR, IMR1 showed the highest value whereas IMR3 had the lowest value (1.66%).

Table 4.3: The percentage difference between normal and abnormal SNR in the four
reconstruction techniques

Percentage difference	IMR1	IMR3	IDOSE2	IDOSE4
Normal SNR	12.13%	17.53%	1.87%	53.99%
Abnormal SNR	11.28%	1.66%	8.93%	6.88%

4.3 Evaluation for patients with fatty liver disease

Table 4.4. shows the mean and standard deviation of abnormal SNR and abnormal CNR for patients with fatty liver disease, for different reconstruction algorithms with 70 and 120 keV tube voltage. In the abnormal area, the SNR for IMR3 reconstruction showed the highest value for both energies. While SNR with IDOSE2 with 70 keV showed the lowest value. In abnormal CNR, IDOSE4 with 120 keV showed the highest value (-0.07). In contrast, the lowest value using IMR3 combined with 120 keV (-4.22) has been found.

Table 4.4: Descriptive statistics for various tube voltage and image reconstruction for patients with fatty liver

	70 kvp protocol				120 kvp protocol			
Parameters	IMR1	IMR3	IDOSE2	IDOSE4	IMR1	IMR3	IDOSE2	IDOSE4
Abnormal SNR	16.53±14.74	19.28±8.77	3.5±1.63	4.12±1.8	10.63±5.35	22.6±9.2	3.62±1.82	4.25±1.64
Abnormal CNR	-1.40±3.66	-1.75±8.98	-0.63±1.42	-0.85±1.88	-0.55±3.06	-4.22±10.89	-0.5±1.28	-0.07±1.41

The percentage difference of abnormal CNR for different reconstructions in patients diagnosed with fatty liver is shown in Table 4.5. The IMR1 was more prominent than other types of imaging reconstruction (43.45%), on the other hand, the IDOSE4 showed the lowest percentage difference (3.11%).

Table 4.5: The percentage difference of abnormal CNR in the four reconstruction techniques in fatty liver patients.

Percentage difference for	IMR1	IMR3	IDOSE2	IDOSE4
Abnormal SNR	43.45%	15.85%	3.37%	3.11%

4.4 Image Quality Evaluation Based on Radiologist

Table 4.6 illustrates the mean and SD of output results obtained from three radiologists' assessments based on 8 reconstructed images with different energy combinations. Based on the assessment, reader 1 has selected IMR3 with a combination with 70 keV as the best image in visibility (4.56±0.63) whereas the IDOSE2 with 120 keV had the lowest image quality (1.56±0.63). The second reader selected IDOSE2 with 120 keV as the best image quality (4.44±0.63) and the IMR3 with 120 keV was the worst image quality based on reader evaluation (1.44±0.51).

The third reader has chosen the IMR1-70 keV as the best reconstruction with energy value to diagnose the targeted pathologies (4.56±0.51) while the IMR3-120 keV combination as the worst image quality in diagnosis visibility (2.25±1.07). The average mean value and SD obtained based evaluator's opinion have shown IMR1-70keV has the best visibility in the diagnosis of pathologies (3.58) with an SD of 0.986. On the other hand, the IMR3-120keV has shown the lowest image quality with a mean value of 2.65 and SD of 1.391.

Table 4.6: The mean and standard deviation for the reconstruction techniques with different keV selections based on reader evaluation

Readers	70 kVp protocol				120 kVp protocol			
	IMR1	IMR3	IDOSE2	IDOSE4	IMR1	IMR3	IDOSE2	IDOSE4
Reader 1	3.69±0.48	4.56±0.63	1.81±0.65	2.44±0.63	3.50±0.73	4.25±0.45	1.56±0.63	2.19±0.66
Reader 2	2.50±.52	1.50±0.52	4.44±0.63	3.56±0.51	2.50±0.52	1.44±0.51	4.38±0.72	3.63±0.50
Reader 3	4.56±0.51	2.44±1.21	2.56±0.73	2.63±0.81	4.38±0.62	2.25±1.07	2.31±0.79	2.75±1

Table 4.7: The averaged mean value and standard deviation for all interrater evaluations in SDCT.

Parameters	Mean	Std. Deviation
IMR1_70kev	3.58	.986
IMR3_70kev	2.83	1.534
DOSE2_70kev	2.94	1.295
DOSE4_70kev	2.88	.815
IMR1_120kev	3.46	.988
IMR3_120kev	2.65	1.391
DOSE2_120kev	2.75	1.391
DOSE4_120kev	2.85	.945

4.5 Radiation dose measurement evaluation

Table 4.7 provides an in-depth analysis of the average mean values and standard deviations associated with interrater evaluations in Spectral detector CT. It is highlighted that IMR1 at 70 keV exhibits the highest mean value of 3.58, boasting a standard deviation of 0.986. Conversely, IMR3 at 70 keV recorded a mean of 2.83, accompanied by a standard

deviation of 1.534. These comparative findings shed light on the nuances within the data obtained, elucidating key insights into the variability observed across the different spectral detector CT evaluations.

In Table 4.8, the results of CTDIvol and CTDIw are displayed, showcasing the calculations derived from both peripheral and central values as previously mentioned. Following this, the percentage differences were determined from these measurements, revealing a 36.9% variance for CTDIvol and 15.9% for CTDIw.

Table 4.8: The radiation dose measurement based on body phantom

Scan type	CTDIvol	CTDIw
MDCT	278.8	209.1
SDCT	175.78	175.78
Percentage differences	36.9%	15.9%

Chapter Five: Discussion

5.1 Introduction

This study highlights the crucial role of a newly available imaging device in the West Bank, discussing its multitude of advantages, the most significant being the substantial reduction in the radiation dose administered to patients. It is well established that improper adaptation of tube voltage can negatively impact image quality, leading to increased noise levels and a diminished signal-to-noise ratio. Another essential factor in minimizing image noise in CT scans is the use of advanced imaging processing techniques that aid in the reconstruction of high-quality images. This improvement is vital for radiologists, particularly in the accurate diagnosis of liver lesions.

The primary objective of this study was to identify and characterize three prevalent liver diseases while assessing both the diagnostic performance and image quality of spectral detector computed tomography (SDCT) based on varying reconstruction techniques and virtual tube voltage. Additionally, the study aimed to compare the radiation dose associated with SDCT and multi-detector computed tomography (MDCT) to provide insights into their relative safety profiles.

The liver is a commonly affected site for both benign and malignant tumors. In global terms of estimated cancer-related mortality, primary liver cancer ranks second among men and sixth among women (Torre et al., 2015). Benign liver tumors, like hepatic cysts, are fluid-filled pockets within the liver that occur in approximately 2.5% of the population and usually present no symptoms. In contrast, primary malignant tumors such as hepatocellular carcinoma (HCC) and metastatic lesions are more concerning, with a substantial portion (40% to 50%) of individuals diagnosed with a primary malignancy also developing liver metastases. Notably, the liver is frequently a site for the metastasis of cancer from other organs (Sleisenger et al., 2010).

Liver tumors, which has direct implications for appropriate patient management and treatment strategies. Consequently, the ability to accurately assess key parameters of liver disease through noninvasive modalities such as MRI, CT, and ultrasound has become essential (Cogley and Miller, 2014). Such noninvasive biomarkers are urgently needed across various clinical research areas and therapeutic settings to enable longitudinal tracking of diseases during treatment, early disease detection, and the exploration of drug development mimetics.

Conventional CT protocols have evolved with the introduction of detector-based spectral computed tomography (SDCT), an innovative dual-energy CT modality that simultaneously captures both low- and high-energy data using dual-layer detectors. This advanced technology employs projection-space decomposition, generating traditional polyenergetic images and spectral basis images, including material-specific decompositions (such as iodine-only, virtual non-contrast images, and effective atomic number images) tailored to specific clinical needs. Furthermore, one of the key advantages of SDCT is its capability to adjust tube voltage after imaging and during post-reconstruction, leading to optimized image quality.

The clinical applications of these enhanced images are vast, including improved lesion visibility, greater vascular contrast, superior material characterization, artifact reduction, and importantly, decreased radiation exposure (Rassouli et al., 2017).

SDCT capitalizes on the energy-dependent attenuation properties of diverse tissues, similar to earlier dual-energy CT techniques, to enhance tissue differentiation. This methodology provides a more extensive dataset compared to conventional CT, resulting in improved diagnostic capabilities (Fulton and Rajiah, 2018). Specifically, spectral detector

CT imaging has demonstrated superior sensitivities across various diseases, achieving sensitivities of 77% and specificity of 95% compared to traditional imaging techniques (Nagayama et al., 2021).

Several factors influence image quality in CT scanners, which, in turn, boosts the efficiency of SDCT over conventional CT. Notably, the imaging algorithm and tube voltage are two pivotal elements. Before iterative reconstruction (IR) algorithms, which were first clinically introduced in 2009, filtered back-projection (FBP) was the preferred approach for many years. The advent of IR has revolutionized CT imaging practices, leading to advanced algorithms developed by major CT vendors specifically for clinical applications. These have evolved into even more sophisticated reconstruction techniques, such as iDose and IMR (Willemink and Noël, 2019).

Tube voltage also plays a critical role; the relationship between radiation dose and tube voltage is linear, meaning an increase in tube voltage will consequently increase the radiation dose. For instance, reducing tube voltage from 120 kVp to 100 kVp can decrease radiation exposure by approximately 33%, and a reduction to 80 kVp can lead to a 65% decrease in radiation dose (Feldle et al., 2024).

 SDCT technology offers substantial advantages over MDCT by providing comprehensive spectral information to all patients without necessitating additional radiation exposure or pre-selective protocol decisions. The imaging capabilities of SDCT also include full temporal and spatial alignment, with complete field-of-view imaging and minimal rotation times of 0.27 seconds, thus enhancing both patient safety and diagnostic accuracy (Rajiah et al., 2017).

5.2 Relation of Reconstruction Algorithm and Tube Voltage

As presented in Table 4.1, the findings reveal a notable trend: increasing the tube voltage in SDCT while maintaining the same reconstruction algorithm leads to a significant enhancement in image quality. This correlation implies a clear relationship where higher kiloelectronvolts (keV) are associated with improved imaging performance, reinforcing existing evidence documented in the literature review.

Furthermore, a closer examination of the Iterative Model Reconstruction (IMR) technique indicates that varying the level of reconstruction yields higher Pearson correlation coefficients, ranging from moderate to strong positive correlations. This contrasts sharply with the Iterative Dose Reduction (iDose) levels, which exhibit only weak positive correlations. Specifically, the Pearson correlation coefficients for IMR at levels 1 and 3 were reported to be 0.462 and 0.789, respectively, illustrating a strong upward trend in correlation with increased IMR levels. In comparison, the iDose levels show notably lower coefficients: iDose at levels 2 and 4 recorded correlations of 0.291 and 0.390, respectively.

These findings align closely with the research conducted by Iyama et al. (2017), which also assessed the Pearson correlation when comparing IMR with iDose and HIR, in addition to FBP. That study revealed that IMR exhibited the highest correlation coefficient ($r = 0.98$), maintaining a significant advantage over other methods, followed by IMR ($r = 0.88$), FBP ($r = 0.41$), and HIR ($r = 0.33$) (Iyama et al., 2017).

The disparities in performance can be attributed to the underlying assumptions present in the CT systems. FBP and HIR methodologies are based on simplified models, including the linear X-ray beam, point source focal spot, and CT detector cells that respond uniformly. In contrast, the IMR method employs precise system models that generate imaging data that is more accurately aligned with the actual measured projection data.

Consequently, the IMR technique not only enhances image resolution but also improves the repeatability of interobserver assessments related to canal stenosis, while effectively reducing noise. These advantages are strongly corroborated by the results obtained, which further validate the superior efficacy of IMR in producing high-quality imaging.

5.3 Imaging Assessment of Metastatic and Hemangioma Cases

In this section, we delve into the comparative analysis of SNR between normal and abnormal hepatic conditions that are imaged with SDCT, specifically focusing on patients diagnosed with metastatic lesions and hemangiomas. The data indicates that the SNR for abnormal liver tissues is consistently lower than that for healthy liver tissues as referred to (Table 4.2). This disparity is attributed to the inherent characteristics of liver lesions, which often exhibit hypoattenuation properties (Ozaki et al., 2022).

Further observations revealed that liver lesions classified as hypointense demonstrate an improved SNR when imaged at a lower energy level of 70 keV compared to higher levels like 120 kV, across various reconstruction techniques. Quantitative results show that for the IMR1, IMR3, iDose 2, and iDose 4 reconstruction algorithms, the SNR values recorded at 70 keV were 9.93, 21.83, 3.51, and 4.36, respectively. In contrast, the SNR values at a higher energy level of 120 keV were slightly diminished, measuring 8.87, 21.47, 3.21, and 4.07 for the same reconstruction techniques, respectively.

Our study confirms that an increase in SNR can be achieved by decreasing keV for abnormal liver lesions, which the liver parenchyma's heightened attenuation can explain due to iodine uptake during the portal venous phase. This phenomenon, driven by an

improved photoelectric effect, leads to increased attenuation values at lower tube voltages (Robinson et al., 2010). Supporting this result, other research has demonstrated statistically significant differences in image quality between datasets and a marked increase in SNR when comparing imaging at 70 kVp versus 120 kVp (Anzidei et al., 2015).

Another study examines lesions as cysts, healthy tissue, or hypodense metastases. Using iodine maps, 40 keV VMIs, and 70 keV VMIs. According to the study, the accuracy of the 40 keV VMIs was the greatest at 0.899, while the accuracy of the traditional data was 0.854. According to the results, spectral CT data may greatly enhance liver imaging clinical workflow and diagnostic precision (Shapira et al., 2020).

Moreover, it is important to discuss the trend observed in the CNR values for both normal and abnormal liver tissues. In a study conducted, the CNR values were measured at different keV settings and reconstruction levels. The results, as illustrated in Table 4.2, showed that the CNR of normal liver tissues diminishes as the keV increases. This implies that as the energy level of the X-ray beam increases, the ability to differentiate between normal liver tissues and surrounding structures decreases.

However, it was observed that the CNR improves as the level of reconstruction increases, regardless of the keV setting. This indicates that higher reconstruction levels positively correlate with improved CNR, suggesting that utilizing advanced reconstruction techniques can enhance the visibility and distinction of abnormalities within the liver. These findings highlight the importance of considering both keV settings and reconstruction levels when evaluating the CNR in liver imaging.

Harun et al. (2021) conducted an analysis on the effect of iterative reconstruction levels on radiation exposure and image quality in CT pulmonary angiography exams,

concluding that an increase in IR level correlates with an approximate 40% increase in CNR. This performance enhancement in CNR is further magnified by the adoption of lower tube voltage selections, potentially increasing CNR by up to 8%.

Ultimately, a significantly enhanced image quality was obtained by lowering tube voltage while simultaneously increasing the level of iterative reconstruction, leading to notable noise reduction outcomes (Harun et al., 2021). These findings align with the results obtained in observations regarding normal liver CNR, although contrasting results were recorded for abnormal liver CNR, where no improvement was noted. Additionally, there were no observed changes in SNR for abnormal liver cases, diverging from the reported SNR values (Song et al., 2015).

Interestingly, the results indicated a superior performance of the IMR algorithm compared to iDose, regardless of tube voltage variations, suggesting that IMR is more effective at managing noise levels than iDose. This assertion is supported by the findings of Kulkarni et al., who compared IMR with low-dose conventional CT and iDose 4 conventional CT specifically for HCC imaging.

Medina et al. (2019) study looked at how different reconstruction methods, such as IMR, iDose4, and FBP, affected image quality at varying doses of radiation. The results of the researchers using a Catphan 500 phantom showed that IMR reconstructions reduced imagine noise by about 75% and enhanced low-contrast detectability by 50% when compared to both FBP and iDose4. These results demonstrated how well IMR works to improve overall system performance and image quality, and they set a standard for routine quality assurance procedures in the imaging center (Osorioa and Namíasb).

Another study compared the images of two iDose4 and IMR to those of conventional filtered back projection (FBP) to evaluate image quality in CT pulmonary angiography performed with minimized radiation exposure and lowered contrast agent volume. Quantitative research revealed that IMR significantly outperformed the iDose4 algorithm, achieving noise reductions of up to 85% compared to FBP and 66% compared to iDose4. IMR produced the highest CNR estimations, further proving its superiority over FBP and iDose4 in creating sharper images (Laqmani et al., 2016b).

Their conclusions underscored that even when utilizing low-dose multidetector computed tomography (MDCT) scans, the IMR algorithm provides improved resolution and enhanced conspicuity of malignant lesions along with a significant reduction in image noise in comparison to the iDose 4 technique (Kulkarni et al., 2021a). Moreover, the IMR technique proves to be essential in imaging patients with cirrhosis, allowing for scanning at lower radiation doses without compromising image quality.

The IMR3 algorithm, in particular, exhibited superior noise suppression in liver imaging when compared to other reconstruction methodologies (Funama et al., 2014). The resultant image profiles and structural contrasts remained intact in the soft-tissue imaging settings of IMR. Enhanced visibility of anatomical structures was made possible due to the pronounced reduction in image noise around the peripheries of the liver (Funama et al., 2014). Our findings align with the previous observations, showing that all parameters recorded for IMR3 at 70 keV were significantly superior to those at 120 keV for patients with liver metastasis and hemangiomas.

5.4 Evaluation for Patients with Fatty Liver Disease

When assessing patients diagnosed with fatty liver disease, it's important to consider the impact of keV settings on the SNR across different imaging reconstruction algorithms. Notably, for the IMR1 technique, studies indicate a decrease in SNR as the keV increases from 70 to 120 keV. This behavior is in contrast to other reconstruction methods such as IMR3, iDose2, and iDose4, where an increase in keV correlates with an improvement in SNR.

Additionally, the SNR tends to improve when employing higher reconstruction levels across different techniques. Specifically, when comparing the various reconstruction methods in the context of fatty liver disease, IMR techniques generally yield superior SNR values compared to iDose techniques. This trend is similar to findings in the imaging of hemangiomas and metastatic lesions, where IMR reconstructions demonstrate a more favorable performance. Moreover, the impact of the choice of reconstruction technique on image quality is important to consider. Data analysis reveals that IMR3 stands out with a higher image quality relative to its counterparts.

This suggests that the application of IMR3 in imaging for patients with fatty liver disease could enhance diagnostic accuracy and overall image clarity. By optimizing the keV settings and utilizing IMR3, radiologists can potentially improve the quality of imaging for patients with fatty liver disease, aiding in the diagnosis and treatment planning process.

5.5 Evaluation of Image Quality Based on Radiologists' Opinions

In the second segment of this study, an evaluation was conducted involving three experienced radiologists. Their expertise was utilized to provide individual opinions on the optimal diagnosis of liver disease when using different reconstruction techniques. The

opinions of these radiologists are summarized in Table 4.6, which highlights their preferences and observations.

One of the radiologists, referred to as reader number one, expressed a preference for the Iterative Model Reconstruction version 3 (IMR3) technique. They believed that it produced higher image quality compared to the iDose 2 technique. This preference was based on the higher mean value of image quality achieved with IMR3.

To further analyze the performance of different reconstruction methods, the radiologists examined the impact of varying kiloelectronvolt (keV) settings. Interestingly, they found that the images reconstructed at the lowest keV values consistently exhibited superior quality. This observation suggests that lower keV settings contribute to improved image quality, potentially enhancing the accuracy of liver disease diagnoses.

The evaluation of image quality was not only focused on mean values but also considered the standard deviation (SD) of the measurements. Remarkably, the standard deviation was found to be relatively small, indicating that the data points were closely clustered around the mean. This tight clustering suggests that the image quality values obtained from these reconstruction techniques are consistent. This consistency is vital as it enhances the diagnostic reliability of the imaging process, allowing for more accurate and confident liver disease diagnoses.

Overall, this evaluation involving the opinions and observations of three radiologists provides valuable insights into the performance and preferences of different reconstruction techniques in liver disease diagnosis. These findings can contribute to the improvement of clinical practice and the enhancement of patient care in the field of radiology.

Conversely, when comparing results from the second radiologist, it was observed that the quality ratings for images at 70 keV and 120 keV were closely aligned; notably, the iDose 2 received the highest quality rating, while IMR3 was deemed the lowest. Radiologist three's findings were markedly different, revealing that images reconstructed at 70 keV were rated substantially higher than those reconstructed at 120 keV. Despite the varied opinions, it emerged that IMR1 was identified as having the highest image quality, whereas IMR3 was cited as having the poorest quality in this analysis.

The discrepancies in the radiologists' evaluations appear to be primarily influenced by their differing levels of familiarity and experience with the iDose technology versus IMR. The second and third radiologists had significantly more experience with iDose, which colored their preferences and led them to rate it more favorably compared to IMR. Furthermore, it is crucial to recognize the impact of each radiologist's expertise on the diagnostic process; varying levels of specialization and knowledge can result in different interpretations of image quality and performance.

This variability in interpretation poses a significant challenge in radiological assessments. The outcomes of imaging techniques often depend on the subjective characteristics of the observer, highlighting the potential for discrepancies in diagnostic conclusions (Benchoufi et al., 2020). If a radiologist becomes proficient with IMR images, they could potentially lower patient radiation exposure, Due to the noise reduction capabilities of this imaging method, the diagnostic potential of the produced images remains uncompromised.

As illustrated in Table 4.7, an individual comparison of interrater agreements revealed that the IMR1 reconstruction at low doses (70 keV) yielded the highest mean image quality values. The data substantiates that IMR1 reconstruction at reduced radiation doses,

combined with a minimal SD of 0.98, demonstrates superior image quality. Notably, the values for IMR1 at 120 keV were found to be strikingly close to those at 70 keV. In contrast, IMR3 consistently produced the lowest image quality values accompanied by a higher SD, indicating a wider spread of values away from the mean, contributing to greater variability and inconsistency.

To establish a solid foundation concerning radiation dosage, a comparative analysis between the radiation doses administered by Multi-Detector Computed Tomography (MDCT) and Spectral Detector Computed Tomography (SDCT) was performed. Measurements for the Volume CT Dose Index (CTDIvol) and Weighted CT Dose Index (CTDIw) were assessed for both MDCT and SDCT.

The findings revealed that SDCT significantly reduces radiation exposure when compared to traditional MDCT techniques. In the analysis outlined in Table 4.8, the standard tube current typically utilized in MDCT was recorded at 378 mAs, whereas SDCT's tube current was measured at 157 mAs. The percentage difference in CTDIvol between the two imaging systems was calculated to be 36.9%, while CTDIw exhibited a reduction of 15.9%. This indicates a pronounced decrease in radiation doses, aligning with the study's original hypothesis.

From a diagnostic perspective, the contrast associated with liver pathologies can be enhanced through a low kilovolt peak (kVp) CT approach, as it increases x-ray absorption and encourages iodine-related photoelectric interactions. These findings corroborate previous research, which indicates that SDCT can effectively diminish radiation doses in multiphase imaging examinations by eliminating the necessity for non-contrast imaging procedures. Support for these results is further strengthened by the research of Rajiah et al., which demonstrated that SDCT protocols achieve volume CT dose index (CTDIvol) values comparable to those of conventional CT scanners, such as the Philips ICT SP (Rajiah et al., 2017).

Utilizing spectral detectors instead of conventional detectors presents opportunities to minimize radiation exposure, primarily by reducing the need for follow-up imaging or unnecessary repeat studies, as well as potentially omitting specific phases from multiphase research. Similar to other Dual-Energy Computed Tomography (DECT) technologies, SDCT allows for lessening the contrast burden while capitalizing on iodine's heightened attenuation properties at lower energy levels (Rajiah et al., 2017).

Kayal et al. (2019) Study also centered on determining how well a new SDCT scanner performs in identifying different kinds of pancreatic lesions. Images reconstructed using low kiloelectron volt (keV) monoE gave the highest Likert scores for reader confidence and tumor conspicuity, according to the analysis. Though the authors expressed that more research is necessary to confirm its clinical significance in wider populations, the data showed that spectral detector CT dramatically improves the visibility of pancreatic cancers (El Kayal et al., 2019).

Furthermore, as mentioned in similar studies by Yan et al. 2023, the DLCT demonstrated a superior ability to detect lesions, exceeding conventional imaging methods with performance of 100% for lesions greater than 15 mm versus 90.5% for lesions smaller than 15 mm. When it came to tumor conspicuity and margin delineation, DLCT—more especially, the VMI 40 keV, IC map, and Zeff map—performed better than conventional CT in subjective assessments. Since Zeff and IC maps performed noticeably better than VMI 40 keV pictures in these areas, the study further emphasizes the potential utility of these modalities in local staging and aiding in the early detection (Yuan et al., 2023).

5.6 Conclusion

The Single-Detector Computed Tomography (SDCT) system is a compelling imaging modality that serves a critical role in identifying and evaluating a wide range of liver pathologies, particularly liver lesions. This advanced technology notably enhances image quality while simultaneously allowing for a reduction in radiation exposure.

In this study, it was observed significant enhancements in several image quality parameters. Specifically, SNR values for both normal and abnormal liver tissues were markedly improved when utilizing SDCT with low radiation doses and a designated strength of Iterative Reconstruction (IR) level. This indicates that the SDCT not only maintains but enhances diagnostic effectiveness even under lower dose conditions.

Furthermore, the CNR for normal liver tissue also displayed substantial improvements when using SDCT techniques. The overall reduction in radiation dose associated with SDCT was notable, with a decrease of 36.9% in the Volume Computed Tomography Dose Index (CTDIvol) and a reduction of 15.9% in the Weighted Computed Tomography Dose Index (CTDIw). These reductions are significant, as they contribute to safer imaging protocols without compromising the quality of the diagnostic images produced.

Additionally, the application of the IMR algorithm in the SDCT framework provided a notable boost in image quality and conspicuity of tumors. The IMR algorithm was particularly effective in minimizing image noise, which is crucial for accurate assessment and diagnosis. When compared with other reconstruction techniques, the IMR algorithm demonstrates superior performance, suggesting that SDCT represents a promising advancement in liver imaging technologies. Overall, these findings highlight the efficacy of SDCT in delivering high-quality images of liver structures while ensuring patient safety through reduced radiation exposure.

5.7 Clinical Recommendation

Based on this study's findings, the number of patients should be increased, and another pathology of liver diseases should be diagnosed. Healthcare professionals should strongly prioritize the selection of the most suitable imaging device when assessing patients with known liver pathology. It is crucial to consider both the radiation dose parameters, such as tube voltage and tube current, and the choice of reconstruction algorithm used during the imaging process.

In particular, the use of SDCT combined with iterative model reconstruction (IMR) has demonstrated significant promise in the imaging of patients with various liver conditions. This imaging technique can be especially beneficial for assessing liver metastases, hemangiomas, and fatty liver disease due to its enhanced image quality and diagnostic capabilities.

Importantly, SDCT has been shown to deliver a lower radiation dose compared to MDCT scans. This reduction in radiation exposure is a vital consideration in the imaging of this patient population, as it helps to minimize the risk of radiation-related complications while still providing high-quality diagnostic imaging. Therefore, adopting SDCT with IMR for liver imaging could represent a marked improvement in both patient safety and diagnostic efficacy.

5.8 Strength of the study

This study critically examined patients diagnosed with three prevalent liver pathologies, aiming to assess two key indicators: the radiation dose delivered by two different CT imaging devices and the effectiveness of a novel spectral detector integrated within a new CT device, alongside its iterative reconstruction algorithm, in the detection and diagnosis of liver lesions.

Due to the retrospective nature of this study design, potential biases were notably minimized. The researchers did not manipulate the sample in any aspect, whether concerning the patient demographics or the algorithm employed for identifying liver pathologies. The essential data were provided by the participating research institutes, and the collaboration of their staff with the researchers significantly facilitated the acquisition of accurate and reliable information.

This study underscored the critical role of SDCT and showcased its capabilities in reducing radiation doses while optimizing the selection of appropriate reconstruction algorithms. By analyzing varying levels of strength in these algorithms, the study aimed to achieve the highest quality liver imaging for diagnostic purposes, all while minimizing the potentially harmful effects of radiation exposure on patients. The findings advocate for the advancement of imaging technologies in improving diagnostic accuracy and patient safety in liver health assessments.

5.9 Limitation

This study has some limitations. Regarding the number of patients with liver disease, Only the venous phase images were utilized, while the arterial and delayed phases were not included. Additionally, the research focused solely on three liver diseases; further studies are needed to explore the other liver diseases. This would help in selecting the appropriate

reconstruction techniques for each condition, ultimately aiming to reduce the radiation dose for patients and achieve the best possible diagnosis.

From another perspective, evaluating diffuse infiltrative lesions versus large lesions, or another liver pathology, the IMR may have different effects. Although reviewers were blinded from the reconstruction algorithm during the image evaluation process, the IMR images' characteristic plastic aspect raises the possibility of data bias.

The ideal study would have involved scanning the patient for appropriate protocol depending on the pathology, but this would not have been practically achievable because most of these patients scanned accidentally. Additionally, it did not compare the findings with the standard diagnostic images produced by other SDCT scanning systems.

5.10 Future Work

There are several promising research directions and potential future projects aimed at extending the study of the novel SDCT device in the detection and characterization of various liver diseases. These areas of exploration could significantly enhance the understanding and application of this technology.

Comparative Research: a comprehensive analysis comparing the traditional computed tomography (CT) techniques with SDCT is crucial. This research should focus on evaluating key metrics such as sensitivity, specificity, and overall diagnostic efficacy of SDCT. By systematically identifying the strengths and weaknesses of SDCT in comparison to standard CT, researchers can better understand how this advanced imaging modality enhances diagnostic accuracy for liver diseases. This comparative study could also involve a diverse cohort of patients with different types of liver conditions to provide robust data.

Conducting longitudinal studies is essential to monitor patients over extended periods, which can help clarify whether specific liver lesions are benign or malignant. Such studies will not only assess the long-term effectiveness of SDCT in identifying early changes in these lesions but also provide insights into the progression of liver diseases over time. This could be particularly beneficial for high-risk populations, where routine screening protocols can be developed and integrated into clinical practice to facilitate early intervention and improved management of liver cancer.

It is also vital to explore advancements in imaging technology that could further augment the capabilities of SDCT. This includes investigating the implementation of sophisticated image analysis techniques, utilizing artificial intelligence (AI) algorithms, and other innovative computational methods that enhance the sensitivity of CT scanning. By leveraging AI and machine learning, we can potentially improve pattern recognition in CT images, enabling more accurate diagnoses and earlier detection of liver disorders.

Future research should also focus on evaluating the effectiveness of various advanced CT scanner types, such as dual-energy and photon-counting CT systems. These innovative technologies could offer significant improvements in detecting liver disorders while simultaneously reducing the time and burden associated with patient preparation. A thorough investigation into these technologies will be instrumental in establishing optimal protocols that enhance patient comfort and diagnostic yield.

In summary, continuing studies in these areas can significantly improve the understanding of the diagnostic sensitivity of SDCT for identifying liver disorders. The insights gained from such research may lead to enhanced screening protocols and ultimately result in better outcomes for patients suffering from liver diseases.

References

ABDELHAMED, W. & EL-KASSAS, M. 2022. Fibrolamellar hepatocellular carcinoma: a rare but unpleasant event. *World Journal of Gastrointestinal Oncology,* 14**,** 1103.

ADAM, S. Z., RABINOWICH, A., KESSNER, R. & BLACHAR, A. 2021. Spectral CT of the abdomen: Where are we now? *Insights into Imaging,* 12**,** 1-16.

AGRAWAL, S., DHIMAN, R. K. & LIMDI, J. K. 2016. Evaluation of abnormal liver function tests. *Postgraduate medical journal,* 92**,** 223-234.

ALVAREZ, R. E. & MACOVSKI, A. 1976. Energy-selective reconstructions in x-ray computerised tomography. *Physics in Medicine & Biology,* 21**,** 733.

AMBROSE, J. 1973. Computerized trans-verse axial tomography. *Brit. J. Radiol.,* 46**,** 148.

AMMORI, B. J., JENKINS, B. L., LIM, P. C., PRASAD, K. R., POLLARD, S. G. & LODGE, J. P. A. 2002. Surgical strategy for cystic diseases of the liver in a western hepatobiliary center. *World journal of surgery,* 26**,** 462-469.

ANZIDEI, M., DI MARTINO, M., SACCONI, B., SABA, L., BONI, F., ZACCAGNA, F., GEIGER, D., KIRCHIN, M., NAPOLI, A. & BEZZI, M. 2015. Evaluation of image quality, radiation dose and diagnostic performance of dual-energy CT datasets in patients with hepatocellular carcinoma. *Clinical radiology,* 70**,** 966-973.

AZIZADDINI, S. & MANI, N. 2020. Liver imaging.

BAK, S., KIM, J. E., BAE, K., CHO, J. M., CHOI, H. C., PARK, M. J., CHOI, H. Y., SHIN, H. S., LEE, S. M. & KIM, H. O. 2020. Quantification of liver extracellular volume using dual-energy CT: utility for prediction of liver-related events in cirrhosis. *European radiology,* 30**,** 5317-5326.

BEFELER, A. S. & DI BISCEGLIE, A. M. 2002. Hepatocellular carcinoma: diagnosis and treatment. *Gastroenterology,* 122**,** 1609-1619.

BELGHITI, J., CAUCHY, F., PARADIS, V. & VILGRAIN, V. 2014. Diagnosis and management of solid benign liver lesions. *Nature reviews Gastroenterology & hepatology,* 11**,** 737-749.

BENCHOUFI, M., MATZNER-LOBER, E., MOLINARI, N., JANNOT, A.-S. & SOYER, P. 2020. Interobserver agreement issues in radiology. *Diagnostic and interventional imaging,* 101**,** 639-641.

BETTS, J. G., DESAIX, P., JOHNSON, E., JOHNSON, J., KOROL, O., KRUSE, D., POE, B., WISE, J., WOMBLE, M. & YOUNG, K. 2013. Anatomy and physiology. OpenStax. *Rice University: Houston, TX, USA***,** 13.

BOLL, D. T. & MERKLE, E. M. 2009. Diffuse liver disease: strategies for hepatic CT and MR imaging. *Radiographics,* 29**,** 1591-1614.

BORGES, A. P., ANTUNES, C. & CASEIRO-ALVES, F. 2023. Spectral CT: Current Liver Applications. *Diagnostics,* 13**,** 1673.

BRADY, S. L., TROUT, A. T., SOMASUNDARAM, E., ANTON, C. G., LI, Y. & DILLMAN, J. R. 2021. Improving image quality and reducing radiation dose for pediatric CT by using deep learning reconstruction. *Radiology,* 298**,** 180-188.

CHAYTOR, R. J., RAJBABU, K., JONES, P. A. & MCKNIGHT, L. 2016. Determining the composition of urinary tract calculi using stone-targeted dual-energy CT: evaluation

of a low-dose scanning protocol in a clinical environment. *The British journal of radiology,* 89**,** 20160408.

CHERQUI, D., RAHMOUNI, A., CHARLOTTE, F., BOULAHDOUR, H., MEIGNAN, M., FAGNIEZ, P. L., ZAFRANI, E. S., MATHIEU, D., DHUMEAUX, D. & MÉTREAU, J. M. 1995. Management of focal nodular hyperplasia and hepatocellular adenoma in young women: a series of 41 patients with clinical, radiological, and pathological correlations. *Hepatology,* 22**,** 1674-1681.

COGLEY, J. R. & MILLER, F. H. 2014. MR imaging of benign focal liver lesions. *Radiologic Clinics,* 52**,** 657-682.

COLLI, A., FRAQUELLI, M., MASSIRONI, S., COLUCCI, A., PAGGI, S. & CONTE, D. 2007. Elective surgery for benign liver tumours. *Cochrane Database of Systematic Reviews*.

CRAIG, J. R., PETERS, R. L. & EDMONDSON, H. A. 1989. *Tumors of the liver and intrahepatic bile ducts*, Armed Forces Institute of Pathology.

DEMARCO, M. P., SHEN, P., BRADLEY, R. F. & LEVINE, E. A. 2006. Intraperitoneal hemorrhage in a patient with hepatic focal nodular hyperplasia. *The American surgeon,* 72**,** 555-559.

DOERNER, J., HAUGER, M., HICKETHIER, T., BYRTUS, J., WYBRANSKI, C., HOKAMP, N. G., MAINTZ, D. & HANEDER, S. 2017a. Image quality evaluation of dual-layer spectral detector CT of the chest and comparison with conventional CT imaging. *European journal of radiology,* 93**,** 5258.

DOERNER, J., WYBRANSKI, C., BYRTUS, J., HOUBOIS, C., HAUGER, M., HENEWEER, C., SIEDEK, F., HICKETHIER, T., GROßE HOKAMP, N. & MAINTZ, D. 2017b. Intra-individual comparison between abdominal virtual mono-energetic spectral and conventional images using a novel spectral detector CT. *PLoS One,* 12**,** e0183759.

DRENTH, J. P., CHRISPIJN, M., NAGORNEY, D. M., KAMATH, P. S. & TORRES, V. E. 2010. Medical and surgical treatment options for polycystic liver disease 1. *Hepatology,* 52**,** 2223-2230.

EL KAYAL, N., LENNARTZ, S., EKDAWI, S., HOLZ, J., SLEBOCKI, K., HANEDER, S., WYBRANSKI, C., MOHALLEL, A., EID, M. & GRÜLL, H. 2019. Value of spectral detector computed tomography for assessment of pancreatic lesions. *European journal of radiology,* 118**,** 215-222.

ERDOGAN, D., BUSCH, O. R., VAN DELDEN, O. M., TEN KATE, F. J., GOUMA, D. J. & VAN GULIK, T. M. 2006. Management of spontaneous haemorrhage and rupture of hepatocellular adenomas. A single centre experience. *Liver International,* 26**,** 433-438.

EULER, A., PARAKH, A., FALKOWSKI, A. L., MANNECK, S., DASHTI, D., KRAUSS, B., SZUCS-FARKAS, Z. & SCHINDERA, S. T. 2016. Initial results of a single-source dual-energy computed tomography technique using a split-filter: assessment of image quality, radiation dose, and accuracy of dual-energy applications in an in vitro and in vivo study. *Investigative radiology,* 51**,** 491-498.

FELDLE, P., GRUNZ, J.-P., KUNZ, A. S., PANNENBECKER, P., PATZER, T. S., PICHLMEIER, S., SAUER, S. T., HENDEL, R., ERGÜN, S. & BLEY, T. A. 2024. Influence of spectral shaping and tube voltage modulation in ultralow-dose computed tomography of the abdomen. *BMC Medical Imaging,* 24**,** 49.

FLOHR, T. 2013. CT systems. *Current Radiology Reports,* 1**,** 52-63.

FLOHR, T., BRUDER, H., STIERSTORFER, K., PETERSILKA, M., SCHMIDT, B. & MCCOLLOUGH, C. 2008. Image reconstruction and image quality evaluation for a dual source CT scanner. *Medical physics,* 35**,** 5882-5897.

FLOHR, T., STIERSTORFER, K., ULZHEIMER, S., BRUDER, H., PRIMAK, A. & MCCOLLOUGH, C. 2005. Image reconstruction and image quality evaluation for a 64-slice CT scanner with-flying focal spot. *Medical physics,* 32**,** 2536-2547.

FLOHR, T. G., MCCOLLOUGH, C. H., BRUDER, H., PETERSILKA, M., GRUBER, K., SÜB, C., GRASRUCK, M., STIERSTORFER, K., KRAUSS, B. & RAUPACH, R. 2006. First performance evaluation of a dual-source CT (DSCT) system. *European radiology,* 16**,** 256-268.

FULTON, N. & RAJIAH, P. 2018. Abdominal applications of a novel detector-based spectral CT.
Current Problems in Diagnostic Radiology, 47**,** 110-118.

FUNAMA, Y., TAGUCHI, K., UTSUNOMIYA, D., ODA, S., KATAHIRA, K., TOKUYASU, S. & YAMASHITA, Y. 2014. Image quality assessment of an iterative reconstruction algorithm applied to abdominal CT imaging. *Physica Medica,* 30**,** 527-534.

GORE, R. M., THAKRAR, K. H., WENZKE, D. R., NEWMARK, G. M., MEHTA, U. K. & BERLIN, J. W. 2012. That liver lesion on MDCT in the oncology patient: is it important? *Cancer Imaging,* 12**,** 373.

GOWDA, S., DESAI, P. B., HULL, V. V., AVINASH, A. K., VERNEKAR, S. N. & KULKARNI, S. S. 2009. A review on laboratory liver function tests. *The Pan african medical journal,* 3.

GREFFIER, J., VILLANI, N., DEFEZ, D., DABLI, D. & SI-MOHAMED, S. 2023. Spectral CT imaging:
technical principles of dual-energy CT and multi-energy photon-counting CT. *Diagnostic and Interventional Imaging,* 104**,** 167-177.

GROßE HOKAMP, N., ABDULLAYEV, N., PERSIGEHL, T., SCHLAAK, M., WYBRANSKI, C., HOLZ, J. A., STREICHERT, T., ALKADHI, H., MAINTZ, D. & HANEDER, S. 2019. Precision and reliability of liver iodine quantification from spectral detector CT: evidence from phantom and patient data. *European radiology,* 29**,** 2098-2106.

HARUN, H. H., KARIM, M. K. A., ABBAS, Z., SABARUDIN, A., MUNIANDY, S. C., RAZAK, H. R. A. & NG, K. H. 2021. The influence of iterative reconstruction level on image quality and radiation dose in CT pulmonary angiography examinations. *Radiation Physics and Chemistry,* 178**,** 108989.

HE, J., MA, X., WANG, Q., FAN, J. & SUN, Z. 2014. Spectral CT demonstration of the superior mesenteric artery: comparison of monochromatic and polychromatic imaging. *Academic radiology,* 21**,** 364-368.

HEALTHCARE, P. 2011. iDose4 Iterative Reconstruction Technique. Breakthrough in image Quality and Dose Reduction With the 4th Generation of Reconstruction. *Eindhoven: Philips Healthcare***,** 1-6.

HOKAMP, N. G., OBMANN, V. C., KESSNER, R., LAUKAMP, K., PERSIGEHL, T., HANEDER, S. & RAMAIYA, N. 2018. Improved visualization of hypodense liver lesions in virtual monoenergetic images from spectral detector CT: proof of concept in a 3D-printed phantom and evaluation in 74 patients. *European journal of radiology,* 109**,** 114-123.

HONG, S., KIM, J. E., CHO, J. M., CHOI, H. C., WON, J. H., NA, J. B., CHOI, D. S., PARK, M. J., CHOI, H.
Y. & SHIN, H. S. 2022. Quantification of liver extracellular volume using dual-energy CT for ruling out high-risk varices in cirrhosis. *European Journal of Radiology,* 148**,** 110151.

HOSCH, W., STILLER, W., MUELLER, D., GITSIOUDIS, G., WELZEL, J., DADRICH, M., BUSS, S. J., GIANNITSIS, E., KAUCZOR, H. U. & KATUS, H. A. 2012. Reduction of radiation exposure and improvement of image quality with BMI-adapted prospective cardiac computed tomography and iterative reconstruction. *European journal of radiology,* 81**,** 3568-3576.

IYAMA, Y., NAKAURA, T., IYAMA, A., KIDOH, M., KATAHIRA, K., ODA, S., UTSUNOMIYA, D. & YAMASHITA, Y. 2017. Feasibility of iterative model reconstruction for unenhanced lumbar CT. *Radiology,* 284**,** 153-160.

JANG, J. K., JANG, H.-J., KIM, J. S. & KIM, T. K. 2017. Focal fat deposition in the liver: diagnostic challenges on imaging. *Abdominal Radiology,* 42**,** 1667-1678.

KALENDER, W. A., SEISSLER, W., KLOTZ, E. & VOCK, P. 1990. Spiral volumetric CT with single-breathhold technique, continuous transport, and continuous scanner rotation. *Radiology,* 176**,** 181-183.

KAMEL, I. R. & BLUEMKE, D. A. 2003. MR imaging of liver tumors. *Radiologic Clinics,* 41**,** 51-65.

KARAOSMANOGLU, A. D., ONUR, M. R., OZMEN, M. N., AKATA, D. & KARCAALTINCABA, M. Magnetic resonance imaging of liver metastasis. Seminars in Ultrasound, CT and MRI, 2016. Elsevier, 533-548.

KHAWAJA, R. D. A., SINGH, S., GILMAN, M., SHARMA, A., DO, S., POURJABBAR, S., PADOLE, A., LIRA, D., BROWN, K. & SHEPARD, J.-A. O. 2014. Computed Tomography (CT) of the Chest at Less Than 1 mSv: An Ongoing Prospective Clinical Trial of Chest CT at Submillisievert Radiation Doses with Iterative Model Image Reconstruction and iDose: 4: Technique. *Journal of computer assisted tomography,* 38**,** 613-619.

KLINGENBECK-REGN, K., SCHALLER, S., FLOHR, T., OHNESORGE, B., KOPP, A. F. & BAUM, U. 1999. Subsecond multi-slice computed tomography: basics and applications. *European journal of radiology,* 31**,** 110-124.

KOU, K., CHEN, Y.-G., ZHOU, J.-P., SUN, X.-D., SUN, D.-W., LI, S.-X. & LV, G.-Y. 2020. Hepatic epithelioid hemangioendothelioma: update on diagnosis and therapy. *World Journal of Clinical Cases,* 8**,** 3978.

KULKARNI, C. B., PULLARA, S. K., PRABHU, N. K., PATEL, S., SURESH, A. & MOORTHY, S. 2021a. Comparison of knowledge-based iterative model reconstruction (IMR) with hybrid iterative reconstruction (iDose4) techniques for evaluation of hepatocellular carcinomas using computed tomography. *Academic Radiology,* 28**,** S29-S36.

KULKARNI, N. M., FUNG, A., KAMBADAKONE, A. R. & YEH, B. M. 2021b. Computed tomography techniques, protocols, advancements, and future directions in liver diseases. *Magnetic Resonance Imaging Clinics,* 29**,** 305-320.

LAMB, P., SAHANI, D. V., FUENTES-ORREGO, J. M., PATINO, M., GHOSH, A. & MENDONÇA, P. R. 2014. Stratification of patients with liver fibrosis using dual-energy CT. *IEEE transactions on medical imaging,* 34**,** 807-815.

LAQMANI, A., AVANESOV, M., BUTSCHEIDT, S., KURFÜRST, M., SEHNER, S., SCHMIDT-HOLTZ, J., DERLIN, T., BEHZADI, C., NAGEL, H. D. & ADAM, G. 2016a. Comparison of image quality and visibility of normal and abnormal findings at submillisievert chest CT using filtered back projection, iterative model reconstruction (IMR) and iDose4™. *European Journal of Radiology,* 85**,** 1971-1979.

LAQMANI, A., KURFÜRST, M., BUTSCHEIDT, S., SEHNER, S., SCHMIDT-HOLTZ, J., BEHZADI, C., NAGEL, H. D., ADAM, G. & REGIER, M. 2016b. CT pulmonary angiography at reduced radiation exposure and contrast material volume using iterative model reconstruction and iDose4 technique in comparison to FBP. *PLoS One,* 11**,** e0162429.

LARBI, A., ORLIAC, C., FRANDON, J., PEREIRA, F., RUYER, A., GOUPIL, J., MACRI, F., BEREGI, J. & GREFFIER, J. 2018. Detection and characterization of focal liver lesions with ultra-low dose computed tomography in neoplastic patients. *Diagnostic and interventional imaging,* 99**,** 311-320.

LAZARIDIS, K. N. & GORES, G. J. 2005. Cholangiocarcinoma. *Gastroenterology,* 128**,** 1655-1667.

LELL, M. M. & KACHELRIEß, M. 2020. Recent and upcoming technological developments in computed tomography: high speed, low dose, deep learning, multienergy. *Investigative radiology,* 55**,** 8-19.

LI, B., YADAVA, G. & HSIEH, J. 2011. Quantification of head and body CTDIVOL of dual-energy x-ray CTwith fast-kVp switching. *Medical physics,* 38**,** 2595-2601.

LI, H., IWAMOTO, Y., HAN, X., LIN, L., HU, H. & CHEN, Y.-W. An accurate unsupervised liver lesion detection method using pseudo-lesions. International Conference on Medical Image Computing and Computer-Assisted Intervention, 2022. Springer, 214-223.

LI, S., YUAN, L., YUE, M., XU, Y., LIU, S., WANG, F., LIU, X., WANG, F., DENG, J. & SUN, Q. 2023. Early evaluation of liver metastasis using spectral CT to predict

outcome in patients with colorectal cancer treated with FOLFOXIRI and bevacizumab. *Cancer Imaging,* 23**,** 1-15.

LI, W., LI, R., ZHAO, X., LIN, X., YU, Y., ZHANG, J., CHEN, K., CHAI, W. & YAN, F. 2021. Differentiation of hepatocellular carcinoma from hepatic hemangioma and focal nodular hyperplasia using computed tomographic spectral imaging. *Journal of clinical and translational hepatology,* 9**,** 315.

MAJEED, N. F., BRASCHI AMIRFARZAN, M., WALD, C. & WORTMAN, J. R. 2021. Spectral detector CT applications in advanced liver imaging. *The British Journal of Radiology,* 94**,** 20201290.

MARIN, D., NELSON, R. C., SAMEI, E., PAULSON, E. K., HO, L. M., BOLL, D. T., DELONG, D. M., YOSHIZUMI, T. T. & SCHINDERA, S. T. 2009. Hypervascular liver tumors: low tube voltage, high tube current multidetector CT during late hepatic arterial phase for detection—initial clinical experience. *Radiology,* 251**,** 771-779.

MARTINS-FILHO, S. N. & PUTRA, J. 2020. Hepatic mesenchymal hamartoma and undifferentiated embryonal sarcoma of the liver: a pathologic review. *Hepatic Oncology,* 7**,** HEP19.

MCCOLLOUGH, C. H., LENG, S., YU, L. & FLETCHER, J. G. 2015. Dual-and multi-energy CT: principles, technical approaches, and clinical applications. *Radiology,* 276**,** 637-653.

MCGLYNN, K. A., PETRICK, J. L. & EL-SERAG, H. B. 2021. Epidemiology of hepatocellular carcinoma. *Hepatology,* 73**,** 4-13.

MCMILLAN, R. R., JAVLE, M., KODALI, S., SAHARIA, A., MOBLEY, C., HEYNE, K., HOBEIKA, M. J., LUNSFORD, K. E., VICTOR III, D. W. & SHETTY, A. 2022. Survival following liver transplantation for locally advanced, unresectable intrahepatic cholangiocarcinoma. *American journal of transplantation,* 22**,** 823-832.

MCNITT-GRAY, M. F. 2002. AAPM/RSNA physics tutorial for residents: topics in CT: radiation dose in CT. *Radiographics,* 22**,** 1541-1553.

MEHTA, D., THOMPSON, R., MORTON, T., DHANANTWARI, A. & SHEFER, E. 2013. Iterative model reconstruction: simultaneously lowered computed tomography radiation dose and improved image quality. *Med Phys Int J,* 2**,** 147-55.

MU, R., MENG, Z., GUO, Z., QIN, X., HUANG, G., YANG, X., JIN, H., YANG, P., ZHANG, X. & ZHU, X. 2022. Dual-layer spectral detector computed tomography parameters can improve diagnostic efficiency of lung adenocarcinoma grading. *Quantitative imaging in medicine and surgery,* 12**,** 4601.

NAGAYAMA, Y., INOUE, T., ODA, S., TANOUE, S., NAKAURA, T., MORINAGA, J., IKEDA, O. & HIRAI, T. 2021. Unenhanced dual-layer spectral-detector CT for characterizing indeterminate adrenal lesions. *Radiology,* 301**,** 369-378.

NG, Y. S., XI, Y., QIAN, Y., ANANTHAKRISHNAN, L., SOESBE, T. C., LEWIS, M., LENKINSKI, R. & FIELDING, J. R. 2020. Use of spectral detector computed tomography to improve liver segmentation and volumetry. *Journal of computer assisted tomography,* 44**,** 197-203.

NOËL, P. B., FINGERLE, A. A., RENGER, B., MÜNZEL, D., RUMMENY, E. J. & DOBRITZ, M. 2011. Initial performance characterization of a clinical noise–suppressing reconstruction algorithm for mdct. *American Journal of Roentgenology,* 197**,** 1404-1409.

NUYTS, J., DE MAN, B., FESSLER, J. A., ZBIJEWSKI, W. & BEEKMAN, F. J. 2013. Modelling the physics in the iterative reconstruction for transmission computed tomography. *Physics in Medicine & Biology,* 58**,** R63.

OSORIOA, A. & NAMÍASB, M. Acceptance testing of a CT scanner with a knowledge-based iterative reconstruction algorithm.

OZAKI, K., HIGUCHI, S., KIMURA, H. & GABATA, T. 2022. Liver metastases: correlation between imaging features and pathomolecular environments. *Radiographics,* 42**,** 1994-2013.

PARK, H. J., LEE, J. M., PARK, S. B., LEE, J. B., JEONG, Y. K. & YOON, J. H. 2016. Comparison of knowledge-based iterative model reconstruction and hybrid reconstruction techniques for
liver CT evaluation of hypervascular hepatocellular carcinoma. *Journal of computer assisted tomography,* 40**,** 863-871.

PHASE, B. V. 2006. Health risks from exposure to low levels of ionizing radiation. *Washington, DC: The British Institute of Radiology*.

RAJIAH, P., ABBARA, S. & HALLIBURTON, S. S. 2017. Spectral detector CT for cardiovascular applications. *Diagnostic and Interventional Radiology,* 23**,** 187.

RAMIREZ-GIRALDO, J. C., FULD, M., GRANT, K., PRIMAK, A. N. & FLOHR, T. 2015. New approaches to reduce radiation while maintaining image quality in multi-detector-computed tomography. *Current Radiology Reports,* 3**,** 1-15.

RASSOULI, N., ETESAMI, M., DHANANTWARI, A. & RAJIAH, P. 2017. Detector-based spectral CT with a novel dual-layer technology: principles and applications. *Insights into imaging,* 8**,** 589-598. ROBINSON, E., BABB, J., CHANDARANA, H. & MACARI, M. 2010. Dual source dual energy MDCT:
comparison of 80 kVp and weighted average 120 kVp data for conspicuity of hypo-vascular liver metastases. *Investigative radiology,* 45**,** 413-418.

SANFELIPPO, P. M., BEAHRS, O. H. & WEILAND, L. H. 1974. Cystic disease of the liver. *Annals of Surgery,* 179**,** 922.

SAUTER, A. P., SHAPIRA, N., KOPP, F. K., AICHELE, J., BODDEN, J., KNIPFER, A., RUMMENY, E. J. & NOËL, P. B. 2020. CTPA with a conventional CT at 100 kVp vs. a spectral-detector CT at 120 kVp: Comparison of radiation exposure, diagnostic performance and image quality. *European Journal of Radiology Open,* 7**,** 100234.

SEERAM, E. 2015. *Computed tomography: physical principles, clinical applications, and quality control*, Elsevier.

SHAKED, O., SIEGELMAN, E. S., OLTHOFF, K. & REDDY, K. R. 2011. Biologic and clinical features of benign solid and cystic lesions of the liver. *Clinical Gastroenterology and Hepatology,* 9**,** 547562. e4.

SHAPIRA, N., FOKUHL, J., SCHULTHEIß, M., BECK, S., KOPP, F. K., PFEIFFER, D., DANGELMAIER, J., PAHN, G., SAUTER, A. P. & RENGER, B. 2020. Liver

lesion localisation and classification with convolutional neural networks: a comparison between conventional and spectral computed tomography. *Biomedical Physics & Engineering Express,* 6**,** 015038.

SHARMA, D., SUBBARAO, G. & SAXENA, R. Hepatoblastoma. Seminars in diagnostic pathology, 2017. Elsevier, 192-200.

SHEFER, E., ALTMAN, A., BEHLING, R., GOSHEN, R., GREGORIAN, L., ROTERMAN, Y., UMAN, I., WAINER, N., YAGIL, Y. & ZARCHIN, O. 2013. State of the art of CT detectors and sources: a literature review. *Current Radiology Reports,* 1**,** 76-91.

SINGH, S., KALRA, M. K., HSIEH, J., LICATO, P. E., DO, S., PIEN, H. H. & BLAKE, M. A. 2010. Abdominal CT: comparison of adaptive statistical iterative and filtered back projection reconstruction techniques. *Radiology,* 257**,** 373-383.

SLEISENGER, M. H., FELDMAN, M., FRIEDMAN, L. S. & BRANDT, L. J. 2010. Sleisenger & Fordtran's gastrointestinal and liver disease: pathophysiology, diagnosis, management. *(No Title)*.

SO, A. & NICOLAOU, S. 2021. Spectral computed tomography: fundamental principles and recent developments. *Korean Journal of Radiology,* 22**,** 86.

SOESBE, T. C., LEWIS, M. A., XI, Y., BROWNING, T., ANANTHAKRISHNAN, L., FIELDING, J. R., LENKINSKI, R. E. & LEYENDECKER, J. R. 2019. A technique to identify isoattenuating gallstones with dual-layer spectral CT: an ex vivo phantom study. *Radiology,* 292**,** 400-406.

SOFUE, K., TSURUSAKI, M., MILETO, A., HYODO, T., SASAKI, K., NISHII, T., CHIKUGO, T., YADA, N., KUDO, M. & SUGIMURA, K. 2018. Dual-energy computed tomography for non-invasive staging of liver fibrosis: Accuracy of iodine density measurements from contrast-enhanced data. *Hepatology Research,* 48**,** 1008-1019.

SOLOFF, E. V., DESAI, N., BUSEY, J. M., KOPROWICZ, K. M. & SHUMAN, W. P. 2020. Feasibility of wide detector three-pass arterial phase liver CT in patients with cirrhosis: timing of hyperenhancing lesion peak conspicuity. *Abdominal Radiology,* 45**,** 2370-2377.

SONG, J. S., LEE, J. M., SOHN, J. Y., YOON, J.-H., HAN, J. K. & CHOI, B. I. 2015. Hybrid iterative reconstruction technique for liver CT scans for image noise reduction and image quality improvement: evaluation of the optimal iterative reconstruction strengths. *La radiologia medica,* 120**,** 259-267.

SURVARACHAKAN, S., PRASAD, P. J. R., NASEEM, R., DE FRUTOS, J. P., KUMAR, R. P., LANGØ, T., CHEIKH, F. A., ELLE, O. J. & LINDSETH, F. 2022. Deep learning for image-based liver analysis— A comprehensive review focusing on malignant lesions. *Artificial Intelligence in Medicine,* 130**,** 102331.

TENG, T. Z. J., DING, C. S. L. & SHELAT, V. G. 2022. Bile duct adenoma: rare benign liver tumour. *Singapore Medical Journal,* 63**,** 769-770.

THANDRA, K. C., BARSOUK, A., SAGINALA, K., PADALA, S. A., BARSOUK, A. & RAWLA, P. 2021. Epidemiology of non-Hodgkin's lymphoma. *Medical Sciences,* 9**,** 5.

TORO, A., MAHFOUZ, A.-E., ARDIRI, A., MALAGUARNERA, M., MALAGUARNERA, G., LORIA, F., BERTINO, G. & DI CARLO, I. 2014. What is changing in indications and treatment of hepatic hemangiomas. A review. *Annals of hepatology,* 13**,** 327-339.

TORRE, L., SIEGEL, R. & JEMAL, A. 2015. Global cancer facts & figures. *Atlanta: American Cancer Society,* 2.

TSILIMIGRAS, D. I., BRODT, P., CLAVIEN, P.-A., MUSCHEL, R. J., D'ANGELICA, M. I., ENDO, I., PARKS, R. W., DOYLE, M., DE SANTIBAÑES, E. & PAWLIK, T. M. 2021. Liver metastases. *Nature reviews Disease primers,* 7**,** 27.

VERNON, G., BARANOVA, A. & YOUNOSSI, Z. 2011. Systematic review: the epidemiology and natural history of non-alcoholic fatty liver disease and non-alcoholic steatohepatitis in adults. *Alimentary pharmacology & therapeutics,* 34**,** 274-285.

WANG, N., JU, Y., WU, J., LIU, A., CHEN, A., LIU, J., LIU, Y. & LI, J. 2019. Differentiation of liver abscess from liver metastasis using dual-energy spectral CT quantitative parameters. *European Journal of Radiology,* 113**,** 204-208.

WEBB, W. 2006. Introduction to CT of the thorax: chest CT techniques. *Fundamentals of Body CT. 3rd ed. Philadelphia, PA: SaundersElsevier***,** 3-10.

WHEELER, D. A. & EDMONDSON, H. A. 1985. Cystadenoma with mesenchymal stroma (CMS) in the liver and bile ducts. A clinicopathologic study of 17 cases, 4 with malignant change. *Cancer,* 56**,** 1434-1445.

WICHMANN, J. L., HARDIE, A. D., SCHOEPF, U. J., FELMLY, L. M., PERRY, J. D., VARGA-SZEMES, A., MANGOLD, S., CARUSO, D., CANSTEIN, C. & VOGL, T. J. 2017. Single-and dual-energy CT of the abdomen: comparison of radiation dose and image quality of 2nd and 3rd generation dual-source CT. *European radiology,* 27**,** 642-650.

WILLEMINK, M. J. & NOËL, P. B. 2019. The evolution of image reconstruction for CT—from filtered back projection to artificial intelligence. *European radiology,* 29**,** 2185-2195.

XI, I. L., WU, J., GUAN, J., ZHANG, P. J., HORII, S. C., SOULEN, M. C., ZHANG, Z. & BAI, H. X. 2021. Deep learning for differentiation of benign and malignant solid liver lesions on ultrasonography. *Abdominal Radiology,* 46**,** 534-543.

YANG, C., WANG, W., CUI, D., ZHANG, J., LIU, L., WANG, Y. & LI, W. 2023. Deep learning image reconstruction algorithms in low-dose radiation abdominal computed tomography: assessment of image quality and lesion diagnostic confidence. *Quantitative Imaging in Medicine and Surgery,* 13**,** 3161.

YIN, X.-P., GAO, B.-L., LI, C.-Y., ZHOU, H., ZHAO, L., ZHENG, Y.-T. & ZHAO, Y.-X. 2018. Optimal monochromatic imaging of spectral computed tomography potentially improves the quality of hepatic vascular imaging. *Korean Journal of Radiology,* 19**,** 578.

YIN, X.-P., ZUO, Z.-W., XU, Y.-J., WANG, J.-N., LIU, H.-J., LIANG, G.-L. & GAO, B.-L. 2017. The optimal monochromatic spectral computed tomographic imaging plus adaptive statistical iterative reconstruction algorithm can improve the superior mesenteric vessel image quality. *European Journal of Radiology,* 89**,** 47-53.

YU, Y., GUO, L., HU, C. & CHEN, K. 2014. Spectral CT imaging in the differential diagnosis of necrotic hepatocellular carcinoma and hepatic abscess. *Clinical Radiology,* 69**,** e517-e524.

YUAN, J., WANG, Y., HU, X., SHI, S., ZHANG, N., WANG, L., DENG, W., FENG, S.-T., PENG, Z. & LUO, Y. 2023. Use of dual-layer spectral detector computed tomography in the diagnosis of pancreatic neuroendocrine neoplasms. *European Journal of Radiology,* 159**,** 110660.

YUKI, H., ODA, S., UTSUNOMIYA, D., FUNAMA, Y., KIDOH, M., NAMIMOTO, T., KATAHIRA, K., HONDA, K., TOKUYASU, S. & YAMASHITA, Y. 2016. Clinical impact of model-based type iterative reconstruction with fast reconstruction time on image quality of low-dose screening chest CT. *Acta Radiologica,* 57**,** 295-302.

ZHANG, D., LI, X. & LIU, B. 2011. Objective characterization of GE discovery CT750 HD scanner: gemstone spectral imaging mode. *Medical physics,* 38**,** 1178-1188.

ZHAO, L.-Q., HE, W., LI, J.-Y., CHEN, J.-H., WANG, K.-Y. & TAN, L. 2012. Improving image quality in portal venography with spectral CT imaging. *European journal of radiology,* 81**,** 1677-1681.

Appendices

appendix A: IRB Approval

IRB Approval Letter

Study Title: "Radiation Dose Assessment Comparison between Spectral CT and MDCT for Diagnoses of Liver Diseases".

Submitted by: Areej Ahmad Hamami

Date received: 12th June 2024

Date reviewed: 23th June 2024

Date approved: 21th July 2024

Your Study titled "**Radiation Dose Assessment Comparison between Spectral CT and MDCT for Diagnoses of Liver Diseases**" with the code number "**R-2024/A/119/N**" was reviewed by the Arab American University Institutional Review Board - Ramallah and it was approved on the 21th of July 2024.

Sajed Ghawadra, PhD
IRB-R Chairman
Arab American University of Palestine

الجامعة العربية الأمريحية . فلسطين
مجلس اخلاقيات البـحت العلمي - رام الله
IRB-R
ARAB AMERICAN UNIVERSITY-PALESTINE
INSTITUTIONAL REVIEW BOARD - RAMALLAH

General Conditions:
1. Valid for 6 months from the date of approval.
2. It is important to inform the IRB-R with any modification of the approved study protocol.
3. The Bord appreciates a copy of the research when accomplished.

Appendix B: Statistical Analysis

Descriptive statistics for various tube voltage and image reconstruction for patients with metastatic and hemangioma

Reconstruction		N	Minimum	Maximum	Mean	Std. Deviation
70KV, IMR1	NormalSNR	10	5.30	39.40	23.1800	11.29275
	AbnormalSNR	10	1.30	17.50	9.9300	5.44998
	NormalCNR	10	3.50	21.60	10.1390	5.73964
	AbnormalCNR	10	-15.90	6.20	-.4690	6.14839
	Valid N (listwise)	10				
70KV, IMR3	NormalSNR	10	20.60	62.80	38.9200	14.03914
	AbnormalSNR	10	2.60	56.20	21.8250	19.49566
	NormalCNR	10	4.20	39.80	13.6300	11.38635
	AbnormalCNR	10	-7.20	19.80	2.1050	7.86287
	Valid N (listwise)	10				
70KV, IDOSE2	NormalSNR	11	3.80	12.50	7.5609	2.35521
	AbnormalSNR	11	.63	8.40	3.5118	2.02424
	NormalCNR	11	1.20	5.90	4.1545	1.73168
	AbnormalCNR	11	-1.90	2.80	.3182	1.33852
	Valid N (listwise)	11				
70KV, IDOSE4	NormalSNR	10	5.50	18.00	9.6000	3.76858
	AbnormalSNR	10	.68	10.40	4.3580	2.60961
	NormalCNR	10	2.30	6.60	4.6130	1.73029
	AbnormalCNR	10	-3.10	3.10	.2850	1.77044
	Valid N (listwise)	10				
120KV, IMR1	NormalSNR	10	13.00	33.30	20.5300	5.20343

		N	Minimum	Maximum	Mean	Std. Deviation
	AbnormalSNR	10	1.90	20.70	8.8700	5.64290
	NormalCNR	10	2.50	17.50	8.6800	4.80504
	AbnormalCNR	10	-6.60	8.00	.7190	4.51320
	Valid N (listwise)	10				
120KV, IMR3	NormalSNR	10	14.40	83.00	46.4000	19.04591
	AbnormalSNR	10	2.30	56.90	21.4700	16.83113
	NormalCNR	10	3.60	25.85	11.3230	7.68586
	AbnormalCNR	10	-15.20	6.60	-.2300	7.00398
	Valid N (listwise)	10				
120KV, IDOSE2	NormalSNR	9	4.90	14.20	7.4222	2.87436
	AbnormalSNR	9	1.10	8.40	3.2100	2.22669
	NormalCNR	9	2.10	6.00	3.8778	1.39801
	AbnormalCNR	9	-3.20	3.20	-.0067	2.02519
	Valid N (listwise)	9				
120KV, IDOSE4	NormalSNR	10	5.12	85.30	16.7020	24.22193
	AbnormalSNR	10	.50	10.60	4.0700	2.71950
	NormalCNR	10	2.10	8.60	4.5700	2.25243
	AbnormalCNR	10	-2.50	3.90	.5740	1.91407
	Valid N (listwise)	10				

Descriptive statistics for various tube voltage and image reconstruction for patients with fatty liver

Reconstruction		N	Minimum	Maximum	Mean	Std. Deviation
70KV, IMR1	AbnormalSNR	6	2.90	43.30	16.5333	14.74377
	AbnormLCNR	6	-5.40	3.80	-1.4000	3.66224
	Valid N (listwise)	6				
70KV, IMR3	AbnormalSNR	6	6.90	29.80	19.2833	8.76503
	AbnormLCNR	6	-14.30	8.80	-1.7500	8.98059
	Valid N (listwise)	6				
70KV, IDOSE2	AbnormalSNR	6	1.30	6.20	3.5000	1.63340
	AbnormLCNR	6	-2.60	1.00	-.6333	1.42361
	Valid N (listwise)	6				
70KV, IDOSE4	AbnormalSNR	6	1.00	6.00	4.1167	1.79935
	AbnormLCNR	6	-3.90	1.10	-.8500	1.87803
	Valid N (listwise)	6				
120KV, IMR1	AbnormalSNR	6	3.70	19.60	10.6333	5.34740
	AbnormLCNR	6	-4.60	3.80	-.5500	3.05598
	Valid N (listwise)	6				
120KV, IMR3	AbnormalSNR	6	7.90	32.80	22.6000	9.20565
	AbnormLCNR	6	-20.30	8.60	-4.2233	10.88790
	Valid N (listwise)	6				
120KV, IDOSE2	AbnormalSNR	6	1.30	6.10	3.6167	1.82035
	AbnormLCNR	6	-2.60	1.40	-.5000	1.27593
	Valid N (listwise)	6				
120KV, IDOSE4	AbnormalSNR	6	1.90	5.50	4.2500	1.63921
	AbnormLCNR	6	-1.50	1.50	-.0667	1.41233
	Valid N (listwise)	6				

Descriptive Statistics based on reader evaluation

Doctor		N	Minimum	Maximum	Mean	Std. Deviation
Dr 2	IMR1_70kev	16	2	3	2.50	.516
	IMR3_70kev	16	1	2	1.50	.516
	DOSE2_70kev	16	3	5	4.44	.629
	DOSE4_70kev	16	3	4	3.56	.512
	IMR1_120kev	16	2	3	2.50	.516
	IMR3_120kev	16	1	2	1.44	.512
	DOSE2_120kev	16	3	5	4.38	.719
	DOSE4_120kev	16	3	4	3.63	.500
	Valid N (listwise)	16				
Dr 1	IMR1_70kev	16	3	4	3.69	.479
	IMR3_70kev	16	3	5	4.56	.629
	DOSE2_70kev	16	1	3	1.81	.655
	DOSE4_70kev	16	1	3	2.44	.629
	IMR1_120kev	16	3	5	3.50	.730
	IMR3_120kev	16	4	5	4.25	.447
	DOSE2_120kev	16	1	3	1.56	.629
	DOSE4_120kev	16	1	3	2.19	.655
	Valid N (listwise)	16				

Dr 3	IMR1_70kev	16	4	5	4.56	.512
	IMR3_70kev	16	1	5	2.44	1.209
	DOSE2_70kev	16	1	4	2.56	.727
	DOSE4_70kev	16	1	4	2.63	.806
	IMR1_120kev	16	3	5	4.38	.619
	IMR3_120kev	16	1	4	2.25	1.065
	DOSE2_120kev	16	1	4	2.31	.793
	DOSE4_120kev	16	1	4	2.75	1.000
	Valid N (listwise)	16				

		IMR1 70kev	IMR3 70kev	IDOSE2 70kev	IDOSE4 70kev	IMR1 120kev	IMR3 120kev	IDOSE2 120kev
IMR3 70kev	Pearson Correlation	0.403(**)	1					
	P Value	0.004						
IDOSE2 70kev	Pearson Correlation	-0.371(**)	-0.562(**)	1				
	P Value)	0.009	0.000					
IDOSE4 70kev	Pearson Correlation	-0.251	-0.340(*)	0.597(**)	1			
	P Value)	0.085	0.018	0.000				
IMR1 120kev	Pearson Correlation	0.462(**)	-0.033	-0.692(**)	-0.587(**)	1		
	P Value	0.001	0.825	0.000	0.000			
IMR3 120kev	Pearson Correlation	0.123	0.789(**)	-0.792(**)	-0.584(**)	0.306(*)	1	
	P Value	0.406	0.000	0.000	0.000	0.034		
IDOSE2 120kev	Pearson Correlation	-0.745(**)	-0.837(**)	0.676(**)	0.291(*)	-0.271	-0.607(**)	1
	P Value	0.000	.000	0.000	0.045	0.063	0.000	
IDOSE4 120kev	Pearson Correlation	-0.592(**)	-0.824(**)	0.288(*)	0.390(**)	0.005	-0.526(**)	0.667(**)
	P Value	0.000	0.000	0.047	0.006	0.974	0.000	0.000

ملخص الرسالة

مقدمة

تعد القدرة التشخيصية لجهاز الفحص الإشعاعي أمرا بالغ الأهمية لتحسين دقة تشخيص أمراض الكبد. أظهر ابتكار التصوير المقطعي المحوسب للكاشف الطيفي (SDCT) أداء تشخيصيا عاليا في تقييم أمراض الكبد بجودة صورة أفضل مقارنة بأجهزة التصوير المقطعي المحوسب التقليدية. يعد اختيار نوع خوارزمية جهد الأنبوب وإعادة البناء المناسب أمرا بالغ الأهمية للحفاظ على جودة الصورة؛ يمكن أن تؤدي الإعدادات غير الصحيحة إلى زيادة الضوضاء وانخفاض نسبة الإشارة إلى الضوضاء.

قصد

أولا، هدفت هذه الدراسة إلى تقييم الدقة التشخيصية للتصوير المقطعي المحوسب الطيفي. ثانيا، تقييم تحسين جودة الصورة بناء على الفولتية الأنبوبية الافتراضية المختلفة وخوارزميات إعادة البناء لتشخيص أمراض الكبد الشائعة.

أساليب

تدور هذه الدراسة حول تحليل بيانات سابقة. تم فحص ستة عشر مريضًا سابقًا باستخدام تصوير مقطعي طيفي وتم تشخيصهم بأحد الحالات المتعلقة بالكبد التالية: كبد دهني، أورام وعائية، أو آفات نقيليه. تم تقييم جهد الأنبوب الافتراضي وخوارزمية إعادة البناء لتقييم تأثير جهد الأنبوب ونوع الخوارزمية على كفاءة التشخيص لأمراض الكبد في صور التصوير المقطعي الطيفي. أعيد بناء الصور باستخدام خوارزميات مختلفة مثل iDose وIMR بدرجات متنوعة مع جهد أنبوب افتراضي مختلف. قام ثلاثة أخصائيين في الأشعة ذوي الخبرة بتحليل ثماني تركيبات من صور التصوير المقطعي المعاد بناؤها، راجعوا 128 مسحًا من 16 مريضًا.

النتيجة

من بين أمراض الكبد، كانت نسبة الإشارة إلى الضوضاء الأعلى في صور التصوير المقطعي الطيفي التي تم مسحها باستخدام خوارزمية IMR3 في الصور النقلية، وأورام وعائية، وكبد دهني. ومع ذلك، عند تصوير الآفات غير الطبيعية في الكبد، تزداد SNR لجميع تقنيات إعادة البناء مع انخفاض جهد الأنبوب.

استنتاج

لوحظت تحسينات كبيرة في العديد من مقاييس جودة الصورة في SDCT عند استخدام جرعات إشعاعية منخفضة. قوة محددة للبناء التكراري (IR) معززة بشكل كبير لقيم نسبة الإشارة إلى الضوضاء (SNR) لكل من أنسجة الكبد الطبيعية والمرضية.

الكلمات الدالة: أمراض الكبد، التصوير المقطعي المحوسب للكاشف الطيفي، التصوير المقطعي المحوسب متعدد الكاشفات، خوارزميات إعادة البناء ، جرعة التصوير المقطعي المحوسب.